Studies on dynamics of nematic disclination under external force

Takuya Yanagimachi
Doctoral Program in Nano-Science and Nano-Technology

Submitted to the Graduate School of
Pure and Applied Sciences
in Partial Fulfillment of the Requirements
for the Degree of Doctor of Philosophy in
Science

at the
University of Tsukuba

Doctoral Committee

Professor Kazuya Saito
Professor Yasuhiro Tokura
Professor Susumu Okada
Dr. Jun-ichi Fukuda

Acknowledgment

I am deeply grateful to Prof. Kazuya Saito for his kindness and precious discussion about whole part of my investigation. He has given me a chance to study for six years. Dr. Yasuhisa Yamamura has given me a lot of advices about my experiments. I could understand experimental system in more detail because of his advices. Dr. Shigenori Nagatomo has given me honest comments for my investigation. Because of his comments, I could have a lot of hints to review my own investigation. Dr. Mafumi Hishida supported my experiment. My technique for using optical microscope and data processing is due to him a lot.

I am grateful to Dr. Syuma Yasuzuka of Hiroshima Institute of Technology. I received helpful guidance from him about investigations. Some basic ideas of experiments are due to discussions with him.

I acknowledge variable discussion with Dr. Jun-ichi Fukuda of National Institute of Advanced Industrial Science and Technology (AIST), especially about theoretical aspects of this work. He gave me a lot of important information about previous investigations. I feel grateful to Prof. Robert Pełka for fruitful discussions. He told me about his theoretical investigation of disclination dynamics during my stay at Institute for Nuclear Physics, Polish Academy of Sciences (PAN).

Needless to say, I feel grateful to students in Saito laboratory. Because of their rapierlike jokes and scientific discussion, I have a pleasant research life.

I am grateful to Dow Corning Toray Co., Ltd. for supplying the vertical alignment material written in Chapter 4. The alignment material (Z-6341 silane) was supplied through their good offices.

This work was supported in part by Basic Research Support Program Type A to T. Yanagimachi from University of Tsukuba.

Contents

Chapter 1

General Introduction

1.1 Disclination in nematic liquid crystal

Most organic materials undergo phase transition with increasing or decreasing temperature. In the case of a phase transition from solid (fully ordered crystal) to liquid, orders of molecular direction and position disappear at the same time. However this is not always the case. When a molecule comprising the system has anisotropic shape (such as rod or disk), some mesophases emerge between the solid and liquid states. The mechanical and symmetrical properties of the state are intermediate between the solid and the liquid. The new phases having fluidity are called liquid crystals (LC) [1, 2].

Because of the anisotropic shape of molecules, LC has the order of molecular orientation, while the order of molecular position is lost. A nematic liquid crystal (NLC) is the simplest case. The molecular order in NLC is schematically shown in Fig. 1.1. The molecular center of gravity is completely disordered in this state. In spite of of thermal fluctuations of molecules, their mean direction of molecules can be defined. A unit vector along the mean direction of molecules is called *director*, written as $\boldsymbol{n}$. If the LC is not ferroelectric, $\boldsymbol{n}$ and $-\boldsymbol{n}$ are indistinguishable. This property of the director is often represented as "headless". NLCs treated in this thesis are not ferroelectric. The headless nature is assumed hereafter, accordingly.

Director is defined as a function of position. In this sense, director forms a kind of field, *director field*. Ideally, the director field should be uniform. However, when the director field extends for a long distance, it may be deformed, resulting in the increase in free energy. Then, lines, the tangent to which coincides with the orientation of the director at the point, can be imagined, similarly to electrical flux lines in electromagnetism. Assuming the smooth variation of the orientation of the director, the director field lines should be continuous. Thus, a line defect around which the director field lines form a loop can easily be imagined as in Fig. 1.2. This is called *disclination* with a *topological*

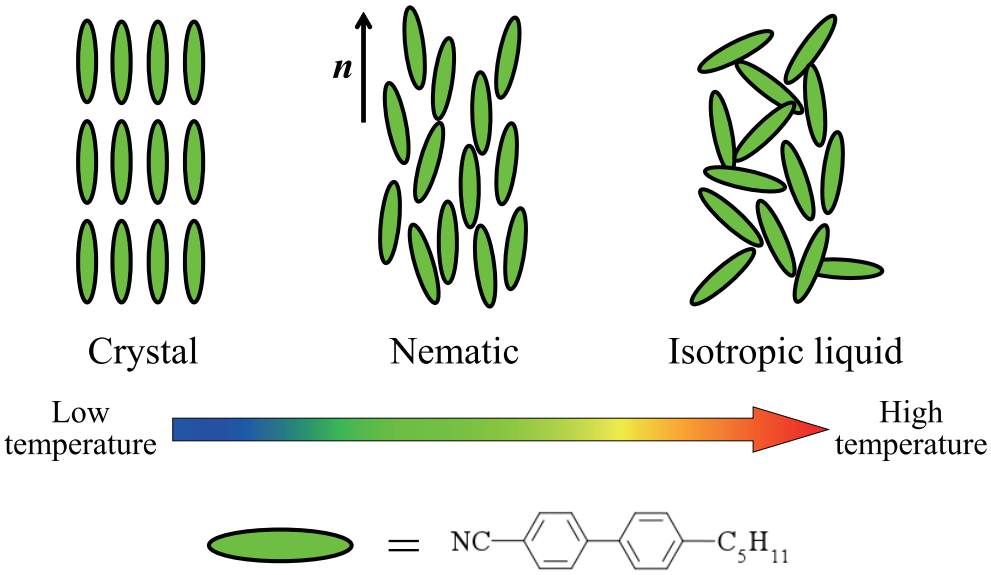

Figure 1.1. Schematic view of molecular order on the course of melting of nematic liquid crystalline compound (nematogen). Molecular structure of 5CB is also shown.

charge $s = 1$ [3, 4]. The director field is deformed largely around the disclination. Nematic order is broken just on the disclination line. This disordered region is called a disclination *core* [1].

The deformation of the director field can be analytically described within an "elastic" theory of a NLC [5], which will be summarized in more detail in Section 1.6. The theory assumes the energy density of the form,

$$f_e = \frac{1}{2}K_1(\nabla \cdot \boldsymbol{n})^2 + \frac{1}{2}K_2(\boldsymbol{n} \cdot (\nabla \times \boldsymbol{n}))^2 + \frac{1}{2}K_3(\boldsymbol{n} \times (\nabla \times \boldsymbol{n}))^2, \tag{1.1}$$

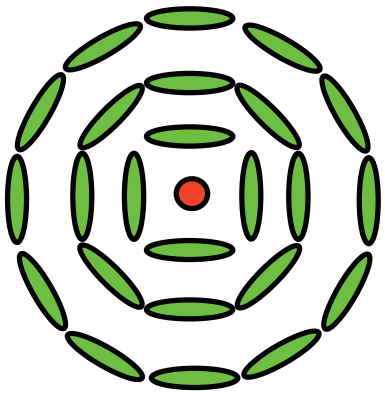

Figure 1.2. Director field around a disclination with $s = 1$.

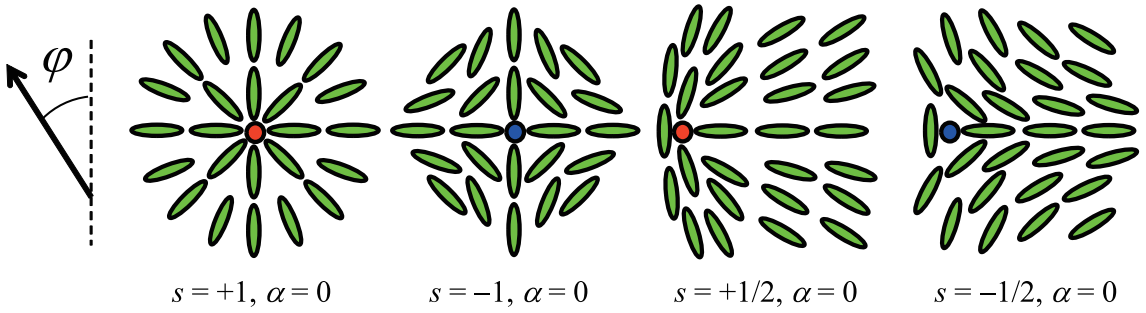

Figure 1.3. Director field represented by representative molecules around kinds of disclinations. φ is an angle of the director.

with K_1, K_2 and K_3 being relevant elastic constants. The liquid crystal is treated as a continuum elastic material while molecular dynamics and its flow are not considered. The director field in the stationary state is described based on the least-energy principle. Hereafter we discuss a two dimensional system of the NLC. When the elastic energy is at its local minimum, the angle of the director φ satisfies Laplace equation. In a two-dimensional system, solutions with the form of

$$\varphi(r,\theta) = s\theta + \alpha, \tag{1.2}$$

is possible with $s = 0, \pm\frac{1}{2}, \pm1, \pm\frac{3}{2}, \pm2, \ldots$ Here, φ is the angle between director and y-axis, which can be taken arbitrarily, and a parameter α is an integral constant. Solutions with non-zero s represent disclinations with idealized symmetry. The topological charge s means the rotation angle of the orientation of director upon turning around a disclination, and the angle is normalized by 2π. The director field is schematically shown in Fig. 1.3 [1] for different s's. It is emphasized that disclinations with a half integer s are allowed because of the headless nature of the director in the case of the NLC, in addition to vortices with non-zero integer s possible for vector fields. Disclinations have been regarded as representative examples of topological defects.

1.2 Annihilation of disclination pair

Because of the deformation of the director field, the elastic energy increases in comparison with the uniformly ordered situation. If the symmetry of the system is not sufficiently high, a disclination moves spontaneously to reduce the elastic energy [6, 7]. The driving force is exerted by the deformed director field around the disclination. The most representative phenomenon is the annihilation of a pair of disclinations [8, 9] having the same magnitude of topological charge but with opposing signs, such

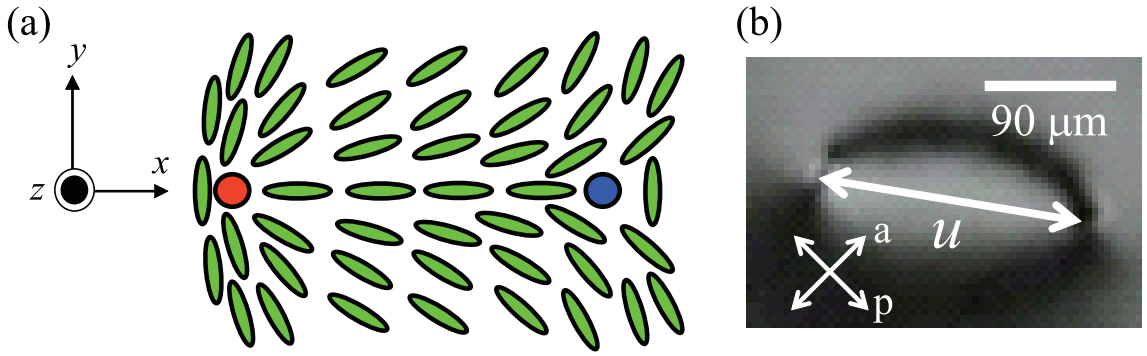

Figure 1.4. $s = \pm 1/2$ disclination pair in NLC. Director field around disclination (a), and image of disclination pair under polarizing optical microscope.

as $s = +\frac{1}{2}$ and $s = -\frac{1}{2}$. A director field around an annihilating disclination pair is schematically shown in Fig. 1.4 (a). Annihilation is widely observed in a NLC sandwiched between glass substrates. This dynamics can be visualized by using a polarizing optical microscope. Observed pairs of disclinations under the crossed Nicols condition is shown in Fig. 1.4 (b). In Fig. 1.4 (b), disclinations are observed as singular points, on which dark and bright lines center. The annihilation of the disclination pairs in (quasi) two-dimensional system has been studied experimentally and theoretically.

The annihilation has successfully been analyzed assuming the balance between elastic driving force and viscous drag [8, 9]. Time evolution of the distance between two annihilating disclinations are theoretically given as

$$u^2 = {u_0}^2 - \frac{2\pi K t}{\Gamma}. \tag{1.3}$$

Here, u is the distance between two disclinations, K is a mean elastic constant of the NLC, and Γ is viscous drag acting on a disclination per unit length. The viscosity Γ had been given theoretically [10, 11] as

$$\Gamma_{\mathrm{theo}} = \frac{\pi}{4}\gamma_{\mathrm{eff}} \ln\left(\frac{3.6\xi_{\mathrm{c}}}{r_{\mathrm{c}}}\right), \tag{1.4}$$

by introducing an effective viscosity γ_{eff} and a core radius r_{c}. A parameter ξ_{c} is a characteristic length [12] that represents the size of the region around disclination where the director field is severely deformed. Annihilation dynamics in the two-dimensional system is described by using this simple theoretical model.

1.3 Anchoring and external field: External force

In the case of a two-dimensional system briefly reviewed in the previous section, only the attractive interaction between two disclinations is considered as a driving force of disclination dynamics. In real systems, however, three-dimensional deformation has to be considered. When the NLC is sandwiched between substrates, molecules are bound to the cell surface. Therefore, the director close to the cell surface does not rotate freely. This anchoring of the director field is called the surface anchoring effect [1, 2]. Because of the anchoring, the additional deformation between the surface area and the inner bulk area is introduced to the NLC system. Bogi *et al.* [12] revealed that this three-dimensional deformation gives additional driving force to the disclinations. In addition, the attractive interaction between disclinations is screened by this. Since the external force due to the anchoring is constant, the disclination moves at a constant velocity as far as the attractive interaction is screened.

Some other additional force can be introduced by applying an external electric field [13, 14]. Disclination dynamics under an external electric field has widely been discussed experimentally and theoretically. The external electric field gives a driving force for a disclination [13] because of the dielectric anisotropy of LC. In general, the dielectric permittivity along the director ($\varepsilon_{\parallel}$) is different from the perpendicular one ($\varepsilon_{\perp}$), resulting in the dielectric anisotropy of the bulk LC [1]. The dielectric anisotropy of the LC is defined as $\varepsilon_{\mathrm{a}} = \varepsilon_{\parallel} - \varepsilon_{\perp}$. When the anisotropy is positive (negative), the director tends to be parallel (perpendicular) to the applied field. Therefore, the director field is deformed under an external electric field [15]. This deformation of the director field influences the driving force acting on a disclination. It is noted that the direction and the magnitude of external force can be controlled by the direction and intensity of the applied field.

Annihilation dynamics was reported for a $s = \pm 1$ disclination pair under an electric field. Minoura *et al.* [13] successfully analyzed the time evolution of the distance u by an elastic theory. They revealed that the external field acts as a phenomenological ordering field on the director field. On the other hand, the case of $s = \pm 1/2$ disclinations was theoretically investigated by Biscari *et al.* [14]. They discussed the effect of external field on single and pair disclination(s) in a two-dimensional infinite system. Dynamics under the field was well discussed in their study. Although they considered the effect of a magnetic field, their result should apply to the electric field.

1.4 Backflow: Spontaneous effect

Flow of the NLC caused by the director reorientation also has a significant effect on the disclination dynamics. Upon the movement of a disclination, the director rotates and the surrounding elastic field changes, accordingly. This rotation of the director is coupled with the velocity field by the so-called *backflow* effect [1, 2]. The effect of the backflow on the movement differs depending on the disclination strength s. The motion of $s = +1/2$ disclinations makes a pair of vortices behind them. The flow points in the direction of defect propagation. The dynamics of $s = +1/2$ disclination is accelerated [16–18] by the vortices pair while the backflow around $s = -1/2$ disclination affects little the movement.

Tóth *et al.* [16] advocated that two sources of flow configure the whole flow field, which influences the disclination motion. One is generated due to the motion of the disclination core. The movement of the core induces a pair of vortices, similar to those following a moving cylinder in an isotropic liquid. This flow is independent of the sign of the disclination. Another flow is generated due to director rotation. The direction of this flow depends on the sign of s, accordingly. These two modes of flow couples, and an asymmetric annihilation is induced. They revealed that $s = +1/2$ disclination is accelerated by the flow, and it moves twice as fast as $s = -1/2$ one. They simulated the flow around $s = \pm 1/2$ disclination pair in a two-dimensional system. The numerically simulated flow field around disclinations is schematically shown in Fig. 1.5. In an experimental way, Blanc *et al.* [18] successfully proved the fact that the asymmetric annihilation is due to the backflow effect. By applying electric field to accelerate disclination, they succeeded to obtain quasi-two dimensional system with negligible surface effects. Their experimental results of asymmetric annihilation were consistent with their theoretical prediction in the two-dimensional system.

1.5 Previous works, motivation, and objects of this thesis

As discussed in the previous sections, notable factors affecting the disclination dynamics consists of three parts: Surface anchoring, external field, and backflow. Surface anchoring and external field gives an external driving force to a disclination. These two effects are experimentally controllable. That is, the strength of the surface anchoring can be controlled by surface treatment process including the choise of an alignment material on the substrate. External electric field is easily controlled by the applied voltage and the frequency, and the gap between electrodes. Even disclination dynamics under a time dependent external force is also observable under the electric field. On the other hand,

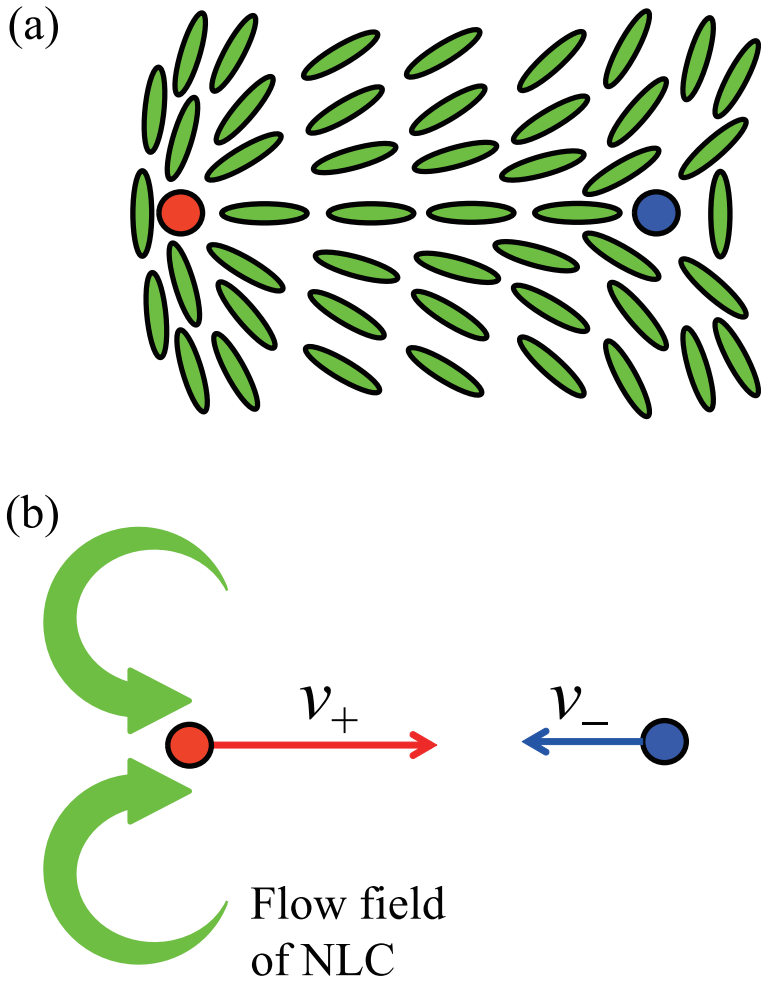

Figure 1.5. Director field around disclination pair (a), and flow field around disclination (b).

backflow is unavoidably accompanied by the disclination dynamics. The backflow is more difficult to control in comparison with two other effects.

Disclination dynamics has been examined experimentally and theoretically in the past. These works are summarized as in Fig. 1.6, which tends not to be a complete list of papers in the past, but to indicate a single representative paper if applicable. Factors exerting some force on a disclination are categorized depending on surface anchoring, external field, and backflow. We think that surface anchoring and external field are especially important for experimental studies because these effects are controllable as an external force acting on a disclination. Figure 1.6 shows that the dynamics under static external force has already been explored [12–14], except for those coupled with backflow. This prompt us to investigate disclination dynamics under the strong anchoring and the external field. Since these three effects can be active simultaneously in real systems, disclination dynamics would become more complicated. Besides, there is no report on the disclination dynamics under time dependent external field as seen in Fig. 1.6. This thesis fills all vacancies in Fig. 1.6.

Chapters 2 and 3 are devoted to experimental studies on the disclination dynamics under stationary force field. The disclination dynamics without an external field is analyzed while considering the backflow effects in Chapter 2. Dependence on the cell gap of the disclination velocity is investigated to explore the anchoring effect. The backflow is taken into consideration. It is revealed that the flow is suppressed near the substrate surfaces because of the anchoring effect.

In Chapter 3, dependence on electric field of the disclination velocity is discussed. Both of the surface anchoring and the electric field influence the disclination dynamics in this system. The disclination velocity is analyzed taking the backflow into account. It is revealed that the backflow is induced in the system, and accelerates $s = +1/2$ disclination even under the electric field as the same extent to that without field.

Chapter 4 describes a study on the disclination dynamics under a time-dependent external force. An abrupt change of the dc voltage is chosen as an example of time-dependent field. A characteristic motion of a disclination, a kind of "damped oscillation", is described in detail. Characteristics of the trajectory of the disclination is discussed and compared with some calculations based on the elastic theory of the NLC.

Experimental findings and their consequences will be summarized in Chapter 5 together with the personal perspective of the author.

The remaining part of this introductory Chapter is devoted to a brief summary of theoretical description of disclination dynamics established in the past.

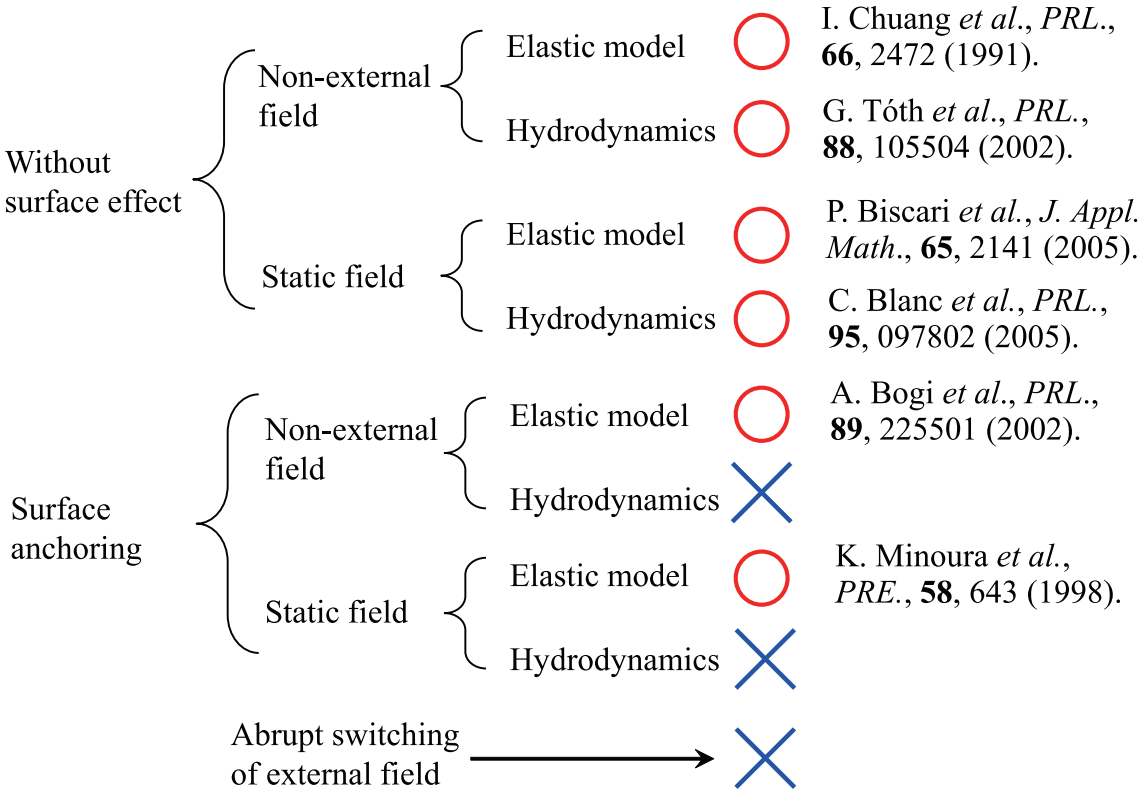

Figure 1.6. Schematic view of previous works.

1.6 Theoretical background

1.6.1 Elastic theory of NLC

Disclination dynamics is described based on the elastic theory. NLC is treated as a continuum medium in this theory. Elastic energy density is written as

$$f_{\mathrm{e}} = \frac{1}{2}K_1(\nabla\cdot\boldsymbol{n})^2 + \frac{1}{2}K_2(\boldsymbol{n}\cdot(\nabla\times\boldsymbol{n}))^2 + \frac{1}{2}K_3(\boldsymbol{n}\times(\nabla\times\boldsymbol{n}))^2. \tag{1.5}$$

Here parameters K_1, K_2 and K_3 are Frank elastic constants [5], corresponding to splay, twist, and bend deformation, respectively. Three deformation modes are schematically shown in Fig. 1.7. More accurately, elastic modulus are written in a tensor form. Sometimes we have to consider a non-diagonal element of the elastic tensor, K_{sb}. K_{sb} is a splay-bend elastic constant, which have an intermediate mode of deformation between the splay and bend modes.

Three elastic constants K_1, K_2 and K_3 are often assumed to be equal for simplicity (one constant approximation). Assuming two-dimensional system, elastic energy density is then written as

$$f_{\mathrm{e}} = \frac{K}{2}(\nabla\varphi)^2. \tag{1.6}$$

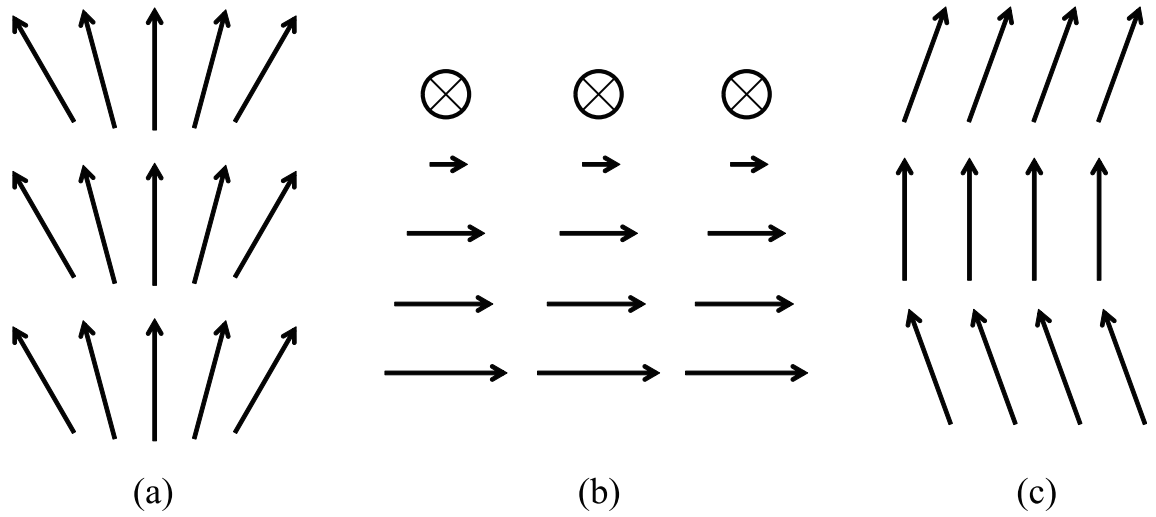

Figure 1.7. Three deformation modes of NLC; splay mode (a), twist mode (b) and bend mode (c).

K is the "mean" elastic constant. The director field in the stationary state is described based on the least-energy principle. When the elastic energy is (local) minimum, the orientation angle φ of director filed satisfies Laplace equation. In two-dimensional systems, some kinds of solutions with the form of Eq. 1.2 are possible as described previously.

Because of the principle of superposition, the director angle φ around the disclinations can be written as follws.

$$\varphi = s_1\theta_1 + s_2\theta_2. \tag{1.7}$$

This equation is written as [2]

$$\varphi = s_1\tan^{-1}(y/x) + s_2\tan^{-1}[y/(x-u)]. \tag{1.8}$$

Equation 1.8 represents the relation between the director angle φ and the position (x, y) in the two-dimensional system. The director at (x, y) is illustrated in Fig. 1.8. A parameter u is the distance between two disclinations. Elastic energy density is given by Eqs. 1.6 and 1.8. Total elastic energy is given as a volume integral of Eq. 1.6. The interaction (force) between disclinations, G_e, is obtained by differentiating the total elastic energy with respect to u. In the case of a disclination pair with $s = \pm 1/2$, an attractive force between two disclinations is written as [6, 8, 9]

$$G_\mathrm{e} = \frac{\pi K d}{2u}. \tag{1.9}$$

A parameter d is the cell gap, which is the distance between upper and lower substrates. Spontaneous

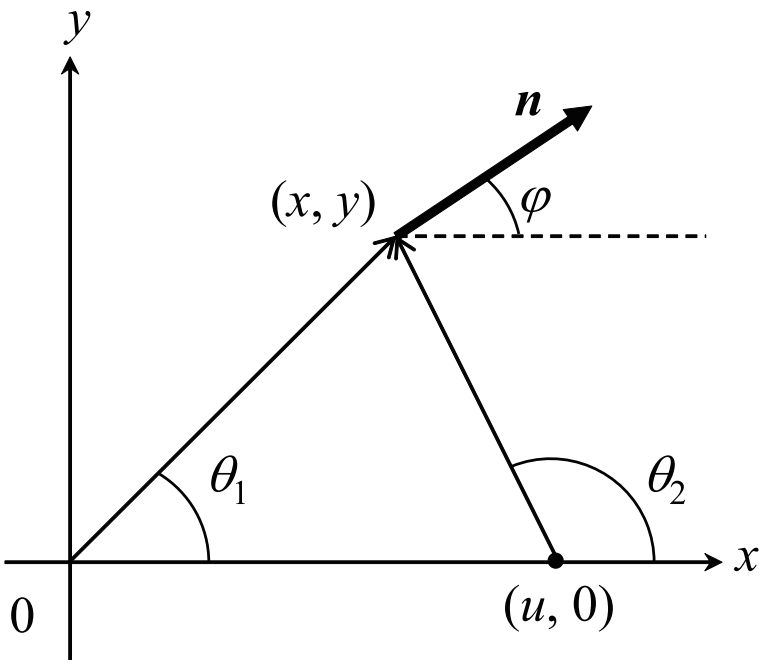

Figure 1.8. Director on the position (x, y). The angle φ is a function of x, y, u, s_1 and s_2.

dynamics of disclinations is usually slow enough [6, 8, 9] that G_e is assumed to balance the viscous drag. Therefore, the time evolution of u is written as the form of Eq. 1.3.

1.6.2 Effect of surface anchoring

Equation 1.3 shows that the distance u is proportional to $t^{1/2}$, and that the disclination velocity depends on time. In real systems, however, u decreases linearly to time for large u [12, 13]. In such a case, the distance u decreases with proportional to $t^{1/2}$ only just before the annihilation. Bogi *et al.* [12] took into consideration the effect of the cell surface. Molecules on the cell surface are fixed, and the rotation of the director is suppressed. This effect is called the surface anchoring. Bogi revealed that the deformation of the director field comes from the surface anchoring generates an additional driving force on a disclination.

A system including $s = \pm 1/2$ pair is schematically shown in Fig. 1.4. Here, x and y axes are set to be parallel to the substrates of sample cell, and z-axis is perpendicular to the surface. The y-axis is set to be parallel to the easy axis of anchoring of the cell surface. Surface of the lower substrate is set to be the origin $z = 0$. Without a disclination, director aligns uniformly. Elastic energy is minimum in this situation. When a disclination pair is introduced to the system, deformation along the z-axis is introduced. This deformation is large in the region between disclination pair (so-called π-wall). Because of the deformation, the elastic energy increases. The director field of π-wall has excess

elastic energy. This excess energy is a function of disclination distance u. Therefore, additional driving force is obtained by differentiating the excess energy with respect to u. The driving force acting on each disclination is written as follows.

$$G_{\text{surface}} = \frac{K_2}{2}\int\left[\left(\frac{\partial\varphi}{\partial z}\right)^2 + \frac{K_{\text{sb}}}{K_2}\left(\frac{\partial\varphi}{\partial y}\right)^2\right]dydz + \frac{K_2}{2L}\int\sin^2\varphi_{\text{s}}dy \tag{1.10}$$

In this equation, φ_{s} is the angle between the director on the cell surface and the anchoring easy axis. L is anchoring extrapolation length, which is the distance between the cell surface and the imaginary position where the director is expected to be parallel to the anchoring easy axis. A parameter l is defined as $l = d + 2L$.

If this system is assumed to be stationary (time-independent), and the director field is decided based on the least-energy principle, the director angle φ should obey Laplace equation. Normalized coordinates are defined as $y' = \sqrt{K_2/K_{\text{sb}}}\frac{\pi}{l}y$ and $z' = \frac{\pi}{l}z$ in the equation.

$$\frac{\partial^2\varphi}{\partial y'^2} + \frac{\partial^2\varphi}{\partial z'^2} = 0. \tag{1.11}$$

Here the boundary condition is as follows:

$$\begin{aligned}
\left.\frac{\partial\varphi}{\partial z'}\right|_{z'=(\pi/2)-(\pi d/2l)} &= \frac{l}{2L\pi}\sin(2\varphi_{\text{s}}),\\
\left.\frac{\partial\varphi}{\partial z'}\right|_{z'=(\pi/2)} &= 0,\\
\left.\frac{\partial\varphi}{\partial y'}\right|_{y'=\pm\infty} &= 0.
\end{aligned}$$

Integration of the Laplace equation under this boundary condition gives the driving force G_{surface} as

$$G_{\text{surface}} = 2\sqrt{K_{\text{sb}}K_2}\left[\frac{\pi}{2} - \text{Tan}^{-1}\left(\frac{L\pi}{l}\right) + \int_0^1 \frac{1}{t}\text{Tan}^{-1}\left(\frac{lt}{L\pi}\right)dt\right]. \tag{1.12}$$

Under the strong anchoring condition, the anchoring extrapolation length L can be taken as 0. Therefore, approximations $L \ll d$ and $l \approx d$ are introduced. Under these approximations, the driving force G_{surface} reads

$$G_{\text{surface}} = 2\sqrt{K_{\text{sb}}K_2}\left[\frac{\pi}{2} - 1 + C + \frac{\pi}{2}\ln\left(\frac{d}{\pi L}\right)\right]. \tag{1.13}$$

Constant C is Catalan's constant defined as

$$C = \int_0^1 \frac{\text{Tan}^{-1}(x)}{x}dx \approx 0.916. \tag{1.14}$$

The total driving force acting on a disclination is the sum of $G_{\rm e}$ and $G_{\rm surface}$. A characteristic length $\xi_{\rm c}$ is defined so that the driving force $G_{\rm e}$ balances to $G_{\rm surface}$ at the distance $u = \xi_{\rm c}$. Now, the total driving force under the strong anchoring condition is written as

$$G_{\rm surface} + G_{\rm e} = G_{\rm surface}(1 + \xi_{\rm c}/u). \tag{1.15}$$

The driving force $G_{\rm e}$ balances $G_{\rm surface}$, i.e., $G_{\rm e} = G_{\rm surface} = \pi K d/(2\xi_{\rm c})$ at $u = \xi_{\rm c}$. $G_{\rm e}$ is screened by $G_{\rm surface}$ when $u \gg \xi_{\rm c}$, accordingly. In this situation, the driving force acting on a disclination is almost constant ($\approx G_{\rm surface}$). Because of this constant driving force, therefore, a disclination moves at a constant velocity. On the other hand, a disclination is accelerated when $u < \xi_{\rm c}$. The attractive interaction between disclinations, $G_{\rm e}$, is large enough, and it increases with decreasing u. The time dependence of u obeys Eq. 1.3 when u becomes short enough.

The viscosity drag $G_{\rm v}$ under zero electric field was discussed by Ryskin *etal* [11]. It is approximately written as

$$G_{\rm v} = \frac{\pi}{4}\gamma_{\rm eff} v \ln\left(\frac{3.6\xi_{\rm c}}{r_{\rm c}}\right). \tag{1.16}$$

Here v is the velocity of a single disclination. Since the velocity of a disclination is assumed to be independent of s within the elastic theory, the relative velocity $-du/dt$ is written as

$$2v = -\frac{du}{dt}. \tag{1.17}$$

A differential equation that describes the time evolution of u is given by this one together with Eq. 1.16.

$$G_{\rm v} = -\frac{\pi}{8}\gamma_{\rm eff} d \ln\left(\frac{3.6\xi_{\rm c}}{r_{\rm c}}\right)\frac{du}{dt} \tag{1.18}$$

Since the disclination motion is assumed to be slow enough, the viscous drag $G_{\rm v}$ balances with the total driving force $G_{\rm surface} + G_{\rm e}$. The time evolution of u under the strong anchoring condition is governed by the following equation [12].

$$\begin{aligned} \frac{du}{dt} &= -v_{\rm asy}\left(1 + \frac{\xi_{\rm c}}{u}\right), \\ v_{\rm asy} t &= u_0 - u + \xi_{\rm c} \ln\left(\frac{u + \xi_{\rm c}}{u_0 + \xi_{\rm c}}\right) \end{aligned} \tag{1.19}$$

A parameter v_{asy} is the asymptotic relative velocity in the region of $u \gg \xi_{\mathrm{c}}$ written as

$$v_{\mathrm{asy}} = \frac{8G_{\mathrm{surface}}}{d\pi\gamma_{\mathrm{eff}}\ln(3.6\xi_{\mathrm{c}}/r_{\mathrm{c}})}. \tag{1.20}$$

Considering the relation $G_{\mathrm{surface}} = \pi Kd/(2\xi_{\mathrm{c}})$, v_{asy} is given by

$$v_{\mathrm{asy}} = \frac{4K}{\gamma_{\mathrm{eff}}\xi_{\mathrm{c}}\ln(3.6\xi_{\mathrm{c}}/r_{\mathrm{c}})}. \tag{1.21}$$

Equation 1.21 shows that the velocity decreases with increasing ξ_{c}.

1.6.3 Dielectric energy

Since LC has dielectric anisotropy, the director field is reoriented depending on an external electric field. Dielectric energy f_{el} is written as [1, 2]

$$f_{\mathrm{el}} = -\frac{1}{2}\varepsilon_0\varepsilon_{\mathrm{a}}(\boldsymbol{E}\cdot\boldsymbol{n})^2. \tag{1.22}$$

Here, parameters $\boldsymbol{E}$, ε_0, and ε_{a} are electric field, permittivity of vacuum, and dielectric anisotropy, respectively. In this research, LC materials 4-cyano-4'-pentylbiphenyl (5CB), the molecular structure of which is shown in Fig. 1.1, and 4-cyano-4'-octylbiphenyl (8CB) are used as samples for experiments. Since 5CB and 8CB have positive dielectric anisotropy, the dielectric energy become minimum when the director $\boldsymbol{n}$ becomes parallel to $\boldsymbol{E}$. The molecular long axis, and consequently the director of the NLC, tends to align parallel to the external electric field.

1.6.4 Frederiks transition

The director aligns parallel to the easy axis of the anchoring under the strong anchoring condition. Without disclinations, the director aligns uniformly in the LC cell. When an external field perpendicularly to the easy axis becomes sufficiently large, the director field is deformed. This deformation has a clear threshold is described as occurrence of Frederiks transition [15]. Figure 1.9 shows the director field before and after the deformation. The easy axis of anchoring is parallel to the surface of this paper, and the electric field perpendicular to it. The director field starts to deform at a threshold field [15]. When the electric field is parallel to the substrates as in Fig. 1.9 (a), the deformation of twist mode is induced. The elastic constant K_2 is relevant to this case, accordingly. The threshold is

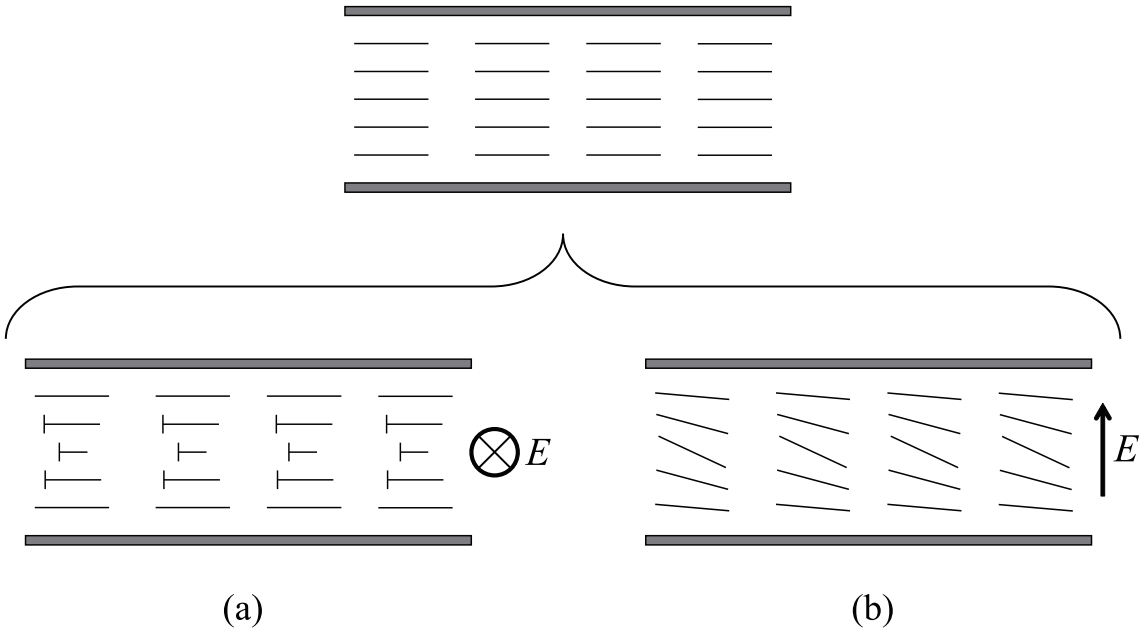

Figure 1.9. Deformation of director field under electric field (Frederiks transition) caused by an applied electric field parallel (a) and normal (b) to the substrates.

given by

$$E_{\mathrm{c}} = \frac{\pi}{d}\sqrt{\frac{K_2}{\varepsilon_0 \varepsilon_{\mathrm{a}}}}. \tag{1.23}$$

If the electric field is applied to perpendicular to the substrates, the director field is deformed as shown in Fig. 1.9 (b). Since bend mode deformation is induced, the elastic constant K_3 is relevant to this case. The threshold electric field is given by

$$E_{\mathrm{c}} = \frac{\pi}{d}\sqrt{\frac{K_3}{\varepsilon_0 \varepsilon_{\mathrm{a}}}}. \tag{1.24}$$

Note that, for geometry (b), the threshold voltage $V_{\mathrm{c}} = E_{\mathrm{c}} d$ is independent of d:

$$V_{\mathrm{c}} = \pi\sqrt{\frac{K_3}{\varepsilon_0 \varepsilon_{\mathrm{a}}}}. \tag{1.25}$$

1.6.5 Flow dynamics of NLC

A NLC flows like a conventional liquid. Since flow dynamics of the NLC couples to the reorientation of director, it becomes more complicated compared to that in isotropic liquids [1, 2].

The flow disturbs the alignment of a director. Conversely, the reorientation of the director induces the flow of the NLC. This flow called backflow [16, 17] influences the dynamics itself.

In order to discuss simultaneously the flow and the elastic energy, a scalar order parameter S and a tensor order parameter $\boldsymbol{Q}$ for the nematic order are introduced. A scalar order parameter S is defined as follows,

$$S = \frac{1}{2}\left(3\langle\cos^2\theta_{\mathrm{m}}\rangle - 1\right). \tag{1.26}$$

Here parameter θ_{m} is an angle between the director $\boldsymbol{n}$ and the molecular long axis. Tensor order parameter is introduced as a function of S, and it is written as

$$Q_{\alpha\beta} = S\left(n_\alpha n_\beta - \frac{1}{3}\delta_{\alpha\beta}\right). \tag{1.27}$$

Indices of $\boldsymbol{Q}$ specify components of Cartesian axis. By using $\boldsymbol{Q}$, the Landau-de Gennes free energy f_{b} and the elastic energy f_{e} are given as [2]

$$f_{\mathrm{b}} = \frac{A}{2}\left(1 - \frac{\Phi}{3}\right)Q_{\alpha\beta}^2 - \frac{A\Phi}{3}Q_{\alpha\beta}Q_{\beta\gamma}Q_{\gamma\alpha} + \frac{A\Phi}{4}(Q_{\alpha\beta}^2)^2, \tag{1.28}$$

$$f_{\mathrm{e}} = \frac{L_1}{2}(\partial_\alpha Q_{\beta\gamma})^2 + \frac{L_2}{2}(\partial_\alpha Q_{\alpha\gamma})(\partial_\beta Q_{\beta\gamma}) + \frac{L_3}{2}Q_{\alpha\beta}(\partial_\alpha Q_{\gamma\varepsilon})(\partial_\beta Q_{\gamma\varepsilon}). \tag{1.29}$$

The parameter Φ is a constant related to a temperature. A represents the relative contribution of the Landau-de Gennes free energy to the total free energy of the system. Parameters L_1, L_2, and L_3 are materials constants related to Frank elastic constants given by

$$L_1 = (K_3 + 2K_2 - K_1)/(9S^2), \tag{1.30}$$

$$L_2 = 4(K_1 - K_2)/(9S^2), \tag{1.31}$$

$$L_3 = 2(K_3 - K_1)/(9S^3), \tag{1.32}$$

Time evolution of the tensor order parameter $\boldsymbol{Q}$ obeys the following equation,

$$(\partial_{\mathrm{t}} + \vec{u}\cdot\nabla)\boldsymbol{Q} - \boldsymbol{S}(\boldsymbol{W},\boldsymbol{Q}) = \Gamma\boldsymbol{H}. \tag{1.33}$$

Here $\vec{u}$ is the velocity of flow in the bulk region, Γ the coefficient of energy dissipation due to the rotation of a director, and $\boldsymbol{W}$ the velocity gradient tensor written as $W_{\alpha\beta} = \partial_\beta u_\alpha = (\partial u_\alpha/\partial x_\beta)$. $\boldsymbol{H}$ in the right hand side is a molecular field for the nematic order, which is related to the free energy F by the following equation.

$$\boldsymbol{H} = -\frac{\delta F}{\delta \boldsymbol{Q}} + \frac{\boldsymbol{I}}{3}\mathrm{Tr}\left(\frac{\delta F}{\delta \boldsymbol{Q}}\right), \tag{1.34}$$

where $\boldsymbol{I}$ is the unit matrix. Function $\boldsymbol{S}(\boldsymbol{W},\boldsymbol{Q})$ is given by

$$\boldsymbol{S}(\boldsymbol{W},\boldsymbol{Q}) = (\xi\boldsymbol{D}+\boldsymbol{\Omega})\left(\boldsymbol{Q}+\frac{\boldsymbol{I}}{3}\right)+\left(\boldsymbol{Q}+\frac{\boldsymbol{I}}{3}\right)(\xi\boldsymbol{D}-\boldsymbol{\Omega})-2\xi\left(\boldsymbol{Q}+\frac{\boldsymbol{I}}{3}\right)\mathrm{Tr}(\boldsymbol{Q}\boldsymbol{W}). \tag{1.35}$$

Here $\boldsymbol{D}$ and $\boldsymbol{\Omega}$ are the symmetric and antisymmetric parts of the velocity gradient tensor, respectively, and ξ a parameter related to the anisotropy of molecular shape.

Velocity of flow in the bulk region $\vec{u}$ obeys Navier-Stokes equation and the elastic theory. Stress tensor exerted on the NLC due to the flow is written as

$$\begin{aligned}\sigma_{\alpha\beta} &= -P_0\delta_{\alpha\beta}-(\xi-1)H_{\alpha\gamma}\left(Q_{\gamma\beta}+\frac{1}{3}\delta_{\gamma\beta}\right)-(\xi+1)\left(Q_{\alpha\gamma}+\frac{1}{3}\delta_{\alpha\gamma}\right)H_{\gamma\beta}\\ &\quad +2\xi\left(Q_{\alpha\beta}+\frac{1}{3}\delta_{\alpha\beta}\right)Q_{\gamma\varepsilon}H_{\gamma\varepsilon}-\partial_\beta Q_{\gamma\nu}\frac{\delta F}{\delta\partial_\alpha Q_{\gamma\nu}}.\end{aligned} \tag{1.36}$$

Parameters P_0 is the pressure. This equation includes terms of the tensor order parameter $\boldsymbol{Q}$ and the molecular field $\boldsymbol{H}$. It shows that the time evolution of order parameter and molecular field generate the stress [2], which induces the flow of the NLC. Namely, disclination dynamics induces macroscopic flow [16, 17].

Chapter 2

Cell gap dependence of asymmetric annihilation

2.1 Introduction

The backflow effect on the annihilation dynamics of disclination pair has been studied by various methods. Numerical simulations ignoring the surface effect have been reported for a two-dimensional system without confinement [16, 17]. These works showed that the backflow makes asymmetric annihilation dynamics. A disclination with $s = +1/2$ moves almost twice as fast as $s = -1/2$ one owing to the backflow. On the other hand, a simple phenomenological model was proposed on the basis of Ericksen-Leslie theory by Sonnet *et al.* [19, 20] A more recent work utilizing perturbative approach [21] explains the mechanism of dissipation around an $s = \pm 1/2$ disclination. The experimental evidence of the backflow effect on disclination dynamics has also been given. Blanc *et al.* [18] observed the electric-field-driven annihilation of nematic disclination pairs with $s = \pm 1/2$ under an electric field which was strong enough for ignoring the effect of cell surfaces. Their experimental setup enabled a quantitative comparison with numerical results.

The fundamental characteristics of the backflow effect have been revealed by considering surface-free systems as briefly summarized above. For more advancement, however, we have to treat the backflow under more realistic situations. It is surmised that a strong anchoring affects the backflow because the surface anchoring suppresses the reorientation of the NLC director.

Effects of cell surfaces on the disclination dynamics and the flow of NLC have been studied theoretically. Denniston [22] showed that the disclination with $s = \pm 1$ requires the flow to move in the medium regardless of the sign. Tóth *et al.* [23] studied the motion of disclination line which is parallel to the substrates. In this situation, the backflow is confined between two cell surfaces.

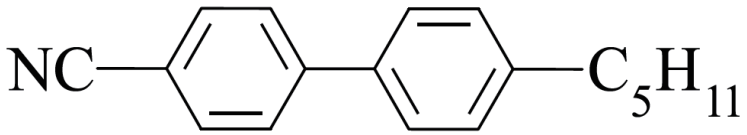

Figure 2.1. Molecular structure of 4-cyano-4'-pentylbiphenyl (5CB).

In this chapter, we study experimentally the annihilation dynamics of disclinations under strong anchoring condition considering backflow effect(s). In order to see the effect of surface systematically, NLC cells were prepared of its thickness distributed in two-order of magnitude ($d = 1 - 92$ μm). We investigate the cell gap dependence of the disclination velocity to reveal the anchoring effect on the dynamics. The velocity ratio v_+/v_- is regarded as a measure of the backflow effect. Cell gap dependence of the velocity ratio was analyzed in order to reveal a mechanism by which the anchoring influences the backflow.

2.2 Experimental

Nematic phase of 4-cyano-4'-pentylbiphenyl (T_{NI} = 35.3 °C) was selected as a sample to study the disclination dynamics, because its material parameters are well known [24, 25]. The material is written as 5CB for short. Structure of the molecule is illustrated in Fig. 2.1.

5CB was sandwiched between two glass plates coated with a homogeneous alignment material. Poly(vinyl alcohol) (PVA) solution (1% in concentration) was used as the homogeneous alignment material. Glass plates were coated with PVA using pieces of paper dipped in PVA solution. The pieces of paper were moved in a particular direction to obtain a strong anchoring condition. The glass plates were then dried. The coating-drying process was performed 8 times. After final drying, the glass plates were heated for 1 h at 130 °C.

The cell gap d was discretely changed by spacers, the thickness of which were 1, 2, 5, 12, 32, 54, and 92 μm. The true cell gap d is expected to be larger than the thickness of spacer by *ca*. 3 μm, which was estimated from separate measurements on cells similarly prepared. The difference between the cell gap and the thickness of spacer scarcely affects the qualitative discussion in this paper.

Disclinations were generated by quenching the sample from $T = 36.0$ °C (isotropic phase) to 34.8 °C (nematic phase) at a rate of 10 K/min. Then the sample temperature was kept constant within

± 0.1 °C by using a hot stage (LINKAM LK-600PM and THMS600) for observation. The image of disclination pairs was recorded through a CCD camera mounted on a polarizing microscope. After the sample was quenched, the dynamics was observed of a disclination pair moving perpendicularly to the anchoring easy axis. As will be described, our setup guarantees the annihilation dynamics of the disclination pair can be discussed while ignoring other disclination(s).

2.3 Results

First we examined the velocity of $\pm 1/2$ disclinations at a constant cell gap ($d = 12$ μm). Two disclinations seemingly moved with constant but different velocities. The velocity was determined by using a least-squares method assuming a linear function of time for their positions. Although the velocity itself depended on cells, which would differ in the strength of surface anchoring, the velocity ratio v_+/v_- for an annihilating pair in each cell remained constant. Since the ratio v_+/v_- is a measure of the backflow, the constant ratio implies that the backflow is not influenced by the strength of surface anchoring if the cell gap is kept constant in our LC cells.

We observed annihilation of disclination pairs with $s = \pm 1/2$ in LC cells with $d = 1 - 92$ μm. Figure 2.2 shows the typical examples of annihilation behaviors. This plot shows the position of two annihilating disclinations with $s = +1/2$ (upper side) and $s = -1/2$ (lower side) as functions of time. Here, we define x as the axis connecting two disclination cores. The asymmetric motion with +1/2 defects moving faster is clearly seen by inspecting the meeting point, which is not halfway between the initial positions of the defects. It is noted that the asymmetry is small in the LC cell with $d = 1$ μm.

Figure 2.2 shows that the motion of disclinations just before annihilation deviates from the linear dependence on time. This trend is more discernible with increasing the cell gap d. In the curved region, the elastic interaction between $\pm 1/2$ disclinations dominates the annihilation [12]. To see this, a characteristic length ξ_c, which is the radius of a cylindrical region (around each disclination core) where the elastic force field associated to the defects dominates the anchoring torque, is calculated. Bogi *et al.* [12] derived the formula of ξ_c within an elastic theory as

$$\xi_c = \frac{\pi K_{sb} d}{4\sqrt{K_{sb} K_2}\left[\frac{\pi}{2} - 1 + C + \frac{\pi}{2}\ln\left(\frac{d}{\pi L}\right)\right]}, \tag{2.1}$$

where K_{sb} and K_2 are, respectively, the splay-bent and twist elastic constants, L the anchoring extrapolation length, and $C = \int_0^1 [\arctan(x)/x]\,dx \approx 0.916$ (Catalan's constant). We set $K_{sb} = 2.4$ pN,

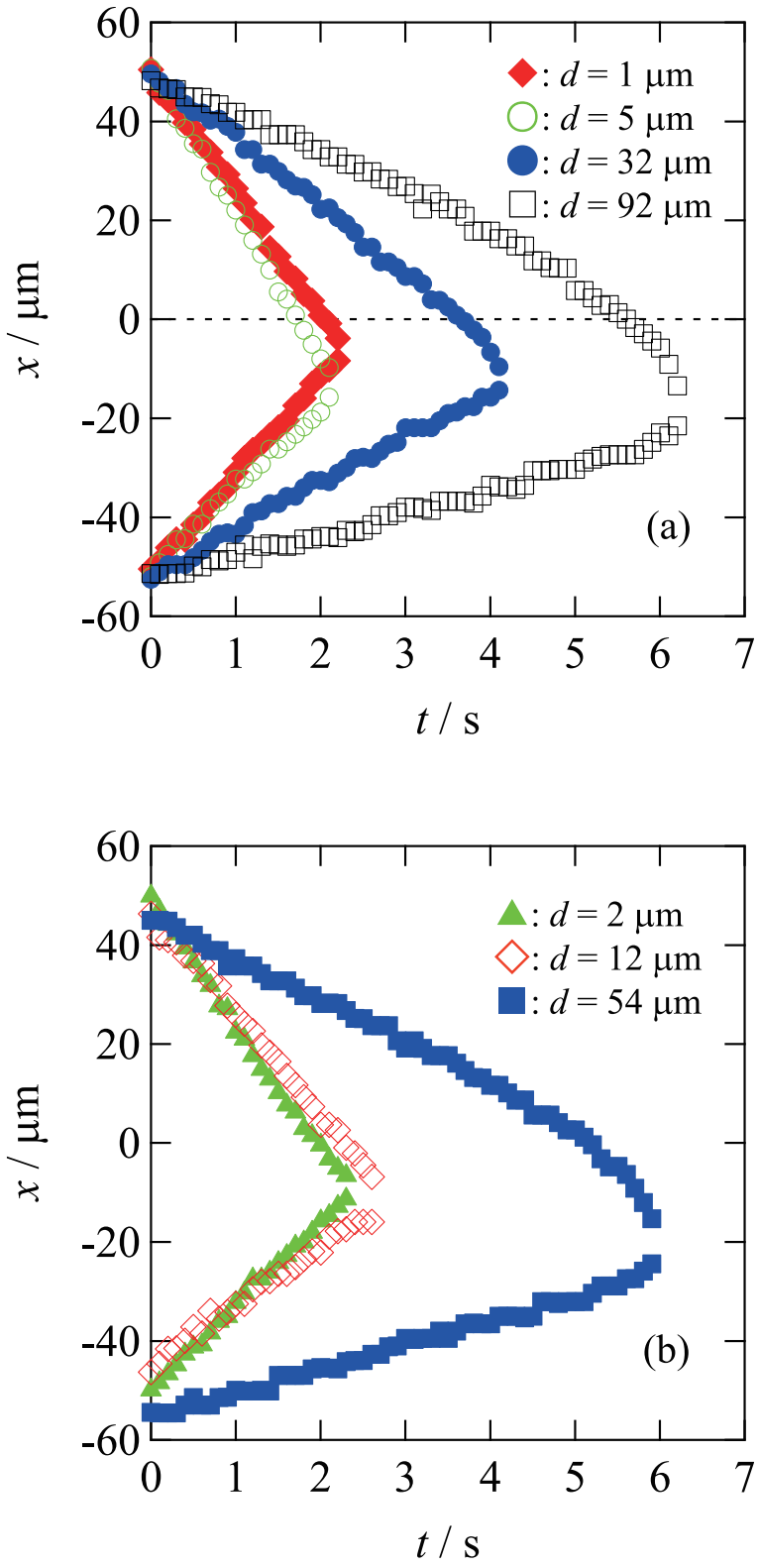

Figure 2.2. Typical annihilation dynamics of $s = \pm 1/2$ disclination pair in LC cells with d =1, 5, 32, and 92 μm (a), and d = 2, 12, and 54 μm (b).

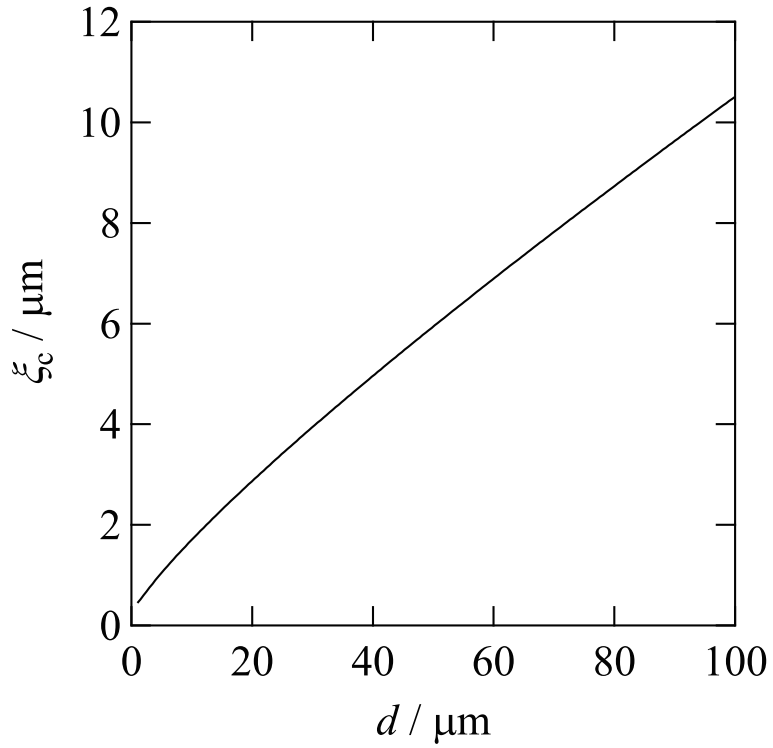

Figure 2.3. Cell gap (d) dependence of ξ_c calculated according to Eq. 2.1.

$K_2 = 1.5$ pN and $L \approx 0.2$ μm [12]. Figure 2.3 shows the dependence of ξ_c on the cell gap d. ξ_c monotonically increases with d. It means that elastic interaction becomes in effect even when the distance between the disclination pair is large in a thicker cell. In other words, the curved region in Fig. 2.2 grows with increasing d. It is noted that ξ_c in Fig. 2.3 is smaller than 10 μm in our experimental setup. The annihilating disclination pairs that we observed were separated from other disclinations at least 30 μm. The disclination pair under observation was safely assumed to behave as if isolated from others.

We define v_+ (v_-) as the velocity of $s = +1/2$ ($-1/2$) disclination in the linear region against time. For $d \leq 12$ μm, we determine v_+ and v_- by applying the least-squares method assuming a linear function of time to the whole course of annihilation dynamics. For $d \geq 32$ μm and larger, however, the curved region is certainly discernible as seen in Fig. 2.2, and should be omitted from the fitting procedure. In order to determine the time domain which we should ignore, we plotted the time dependence of u^2, where u is the distance between the annihilating disclinations. When u is small, u^2 exhibits a linear decrease with time (shown in Fig. 2.4). It means that u obeys the square-root time law [8, 9]. A linear region of a plot like Fig. 2.4 was thus omitted in determining v_+ and v_- by the least-squares analysis assuming a linear function of time.

The validity (adequacy) of our determination of v_+ and v_- was examined from two aspects: 1)

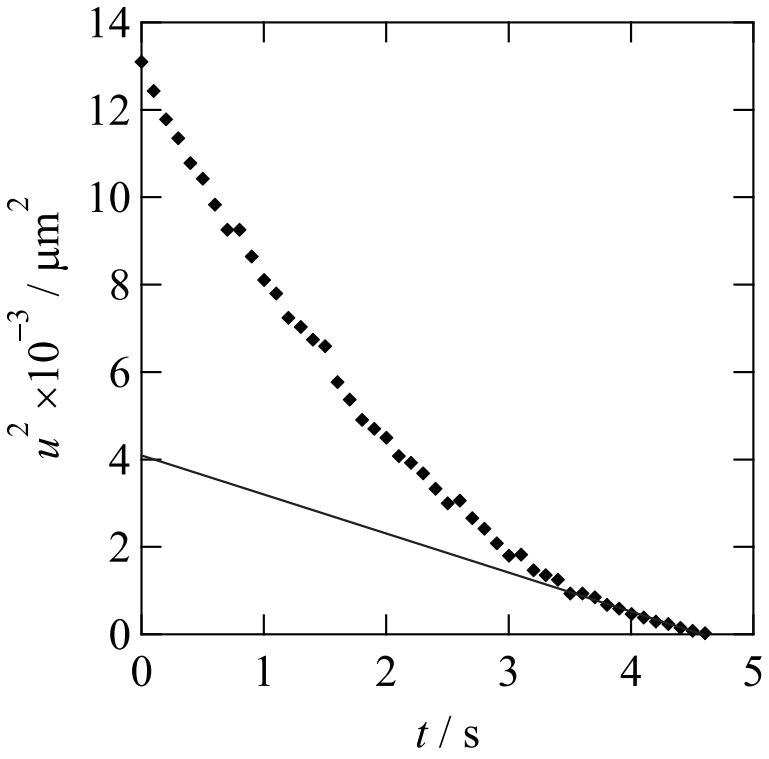

Figure 2.4. Time dependence of u^2. The straight line shows the square-root time law [8, 9] before annihilation.

elastic constant K from Fig. 2.4, and 2) v_- itself in comparison with a theoretical magnitude. First we discuss the elastic constant. When u is small, the defect annihilation is dominated by elastic interaction between the two disclinations, and the effect of the surface anchoring is negligible. u obeys the square-root time law in this situation. If only the elastic interaction between disclinations is considered as a driving force of the annihilation in Eq. 2.2, the time dependence of u without the surface effect is given by [8, 9]

$$u^2 = {u_0}^2 - \frac{8\pi K t}{\pi \gamma_{\rm eff} \ln\left(\frac{3.6\xi_c}{r_c}\right)}, \tag{2.2}$$

where $\gamma_{\rm eff}$ is the effective viscosity expressed as

$$\gamma_{\rm eff} = \gamma_1 - \frac{\alpha_2^2}{2(\eta_b - \gamma_2)} \tag{2.3}$$

in terms of the orientational viscosity γ_1, and coefficients related to the Leslie coefficients (α_2, η_b, and γ_2) [12, 24]. The numerical value of $\gamma_{\rm eff}$ is calculated as 1.1×10^{-2} Pa s. Ten annihilation data yields, in average, $K = 1.5$ pN, which is favorably compared with the reported estimate for 5CB (about $1 - 2$ pN) [25]. Therefore the elastic interaction between disclinations is certainly dominant in the linear region of Fig. 2.4. Second we discuss the experimental magnitude of v_- itself. Since the backflow

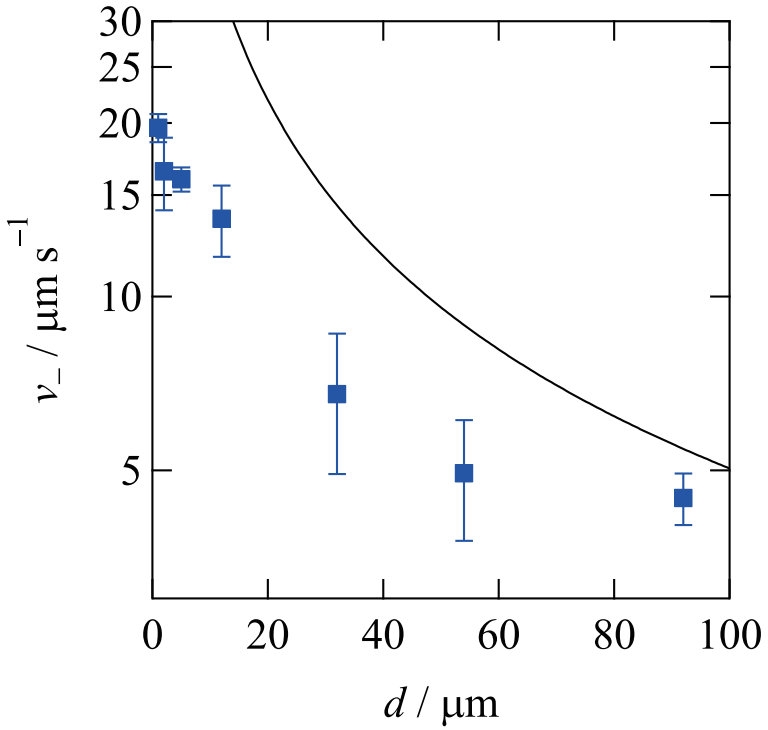

Figure 2.5. Cell gap (d) dependence of experimental v_- and theoretical v while ignoring the backflow effect calculated by using Eq. 2.4.

is very weak around an $s = -1/2$ disclination, v_- is close to the velocity estimated within the elastic theory. In our experiment, only the anchoring energy contributes to the velocity v_-. The driving force from the anchoring energy should be equal to the viscosity [12]. The velocity of an $s = -1/2$ disclination is thus given by

$$v_- = \frac{8\sqrt{K_{sb}K_2}\left[\frac{\pi}{2} - 1 + C + \frac{\pi}{2}\ln\left(\frac{d}{\pi L}\right)\right]}{d\pi\gamma_{eff}\ln\left(\frac{3.6\xi_c}{r_c}\right)}. \tag{2.4}$$

The constant r_c is the radius of the core. We set $r_c = 0.01$ μm considering the literature [12]. The dependence of v_- on cell gap d is shown in Fig. 2.5. The experimental and theoretical velocities are qualitatively consistent. The above analyses show that the determination of v_+ and v_- seems acceptable.

The velocity of a disclination was determined by using the method noted above. The actual value of velocity exhibits difference depending on the position within a cell. Figure 2.6 shows experimental velocities of annihilating disclinations ($d = 54$ μm). The annihilation was observed at three positions in a LC cell. These observations were repeated for more than 20 times at each position. Each point with an error bar means the average of velocity in one position.

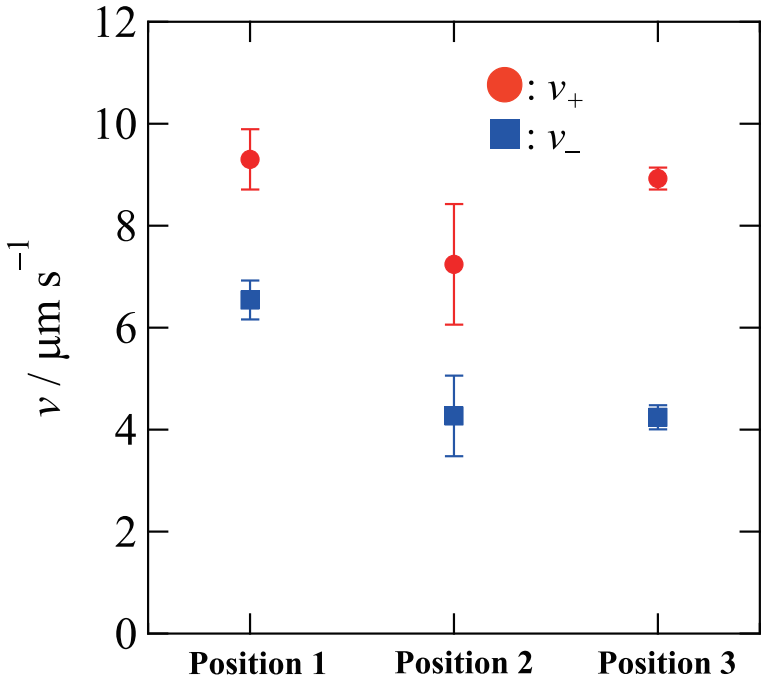

Figure 2.6. The disclination velocity of each position, in the $d =$ 54 μm LC cell.

Having validated the determination of v_+ and v_-, we proceed to the issue of the strength of the backflow effect. Figure. 2.7 shows the relation between v_+/v_- and cell gap d. The largest error bar is exhibited by the $d = 54$ μm cell, the data of which are shown in Fig. 2.6. $v_+/v_- \approx 2$ is expected from theoretical studies ignoring the influence of surfaces. In our experiment, v_+/v_- gets close to 2 with the cell gap d becoming large. This is reasonable because the surface effect becomes relatively small with increasing d. It is emphasized that the velocity ratio v_+/v_- at $d = 1$ μm is much smaller than a smooth (straight) curve in Fig. 2.7. The straight line means a logarithmic function. Figure 2.7 shows that the reduction of v_+/v_- around $d = 1$ μm is more rapid than the logarithmic function. v_+/v_- seems to be changed discontinuously. This implies that $d = 1$ μm LC cell has different flow mode from thicker cells.

2.4 Discussion

Let us discuss the dependence on the cell gap d of the velocity ratio v_+/v_-, which is a measure of the backflow. The elastic anisotropy is ignored in the following, though it could cause asymmetric annihilation of a disclination pair in Langmuir monolayers [26]. Previous theoretical studies [16, 17] predicted $v_+/v_- \approx 2$ in the absence of surfaces. If the backflow is suppressed by cell surfaces, it is expected that v_+/v_- gets close to the unity.

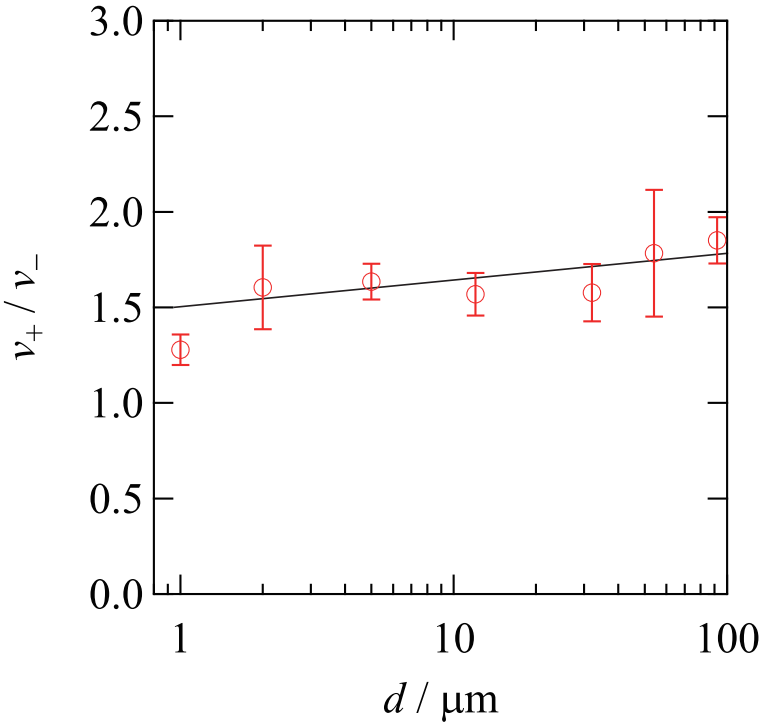

Figure 2.7. Cell gap (d) dependence of velocity ratio v_+/v_-. A straight line is a guide for eyes.

When the cell gap is thicker than 2 μm, the velocity ratio increase slightly with the increase in the cell gap d. The ratio $v_+/v_- \approx 1.8$ is reached at $d = 10^2$ μm as seen in Fig. 2.7. This magnitude is comparable with the theoretical prediction (*ca.* 2). It shows that thicker LC cells have the region where the surface effect could be ignored. This region should locate at the central part of a cell in the direction of thickness, because the surface effect is the weakest there. Figure 2.8 schematically shows the expected distribution of the director field in a thick LC cell. A constant (uniform) flow is expected in the region near the center of the cell. This region is denoted "free flow region" hereafter. On the other hand, Fig. 2.7 shows that v_+/v_- drops sharply when $d = 1$ μm. It means that the backflow is suppressed in the LC cell. A region with weak flow exists near the cell surface. We call this region "suppressed flow region." Considering the fact that NLC is sandwiched between two glass plates, the thickness of the suppressed flow region is about 0.5 μm.

We discuss the mechanism of the backflow to explain the dependence of velocity ratio on cell gap d. Tóth *et al.* [16] showed that the coupling of two modes of flow causes the total backflow. One mode comes from the director rotation involved in the disclination movement. The sense of the director rotation is decided by the sign of s. The other mode comes from the movement of the disclination core, where the nematic order is suppressed. The core can be treated as a moving cylinder in the NLC. The movement of the core induces vortices, accordingly. This mode is independent of disclination

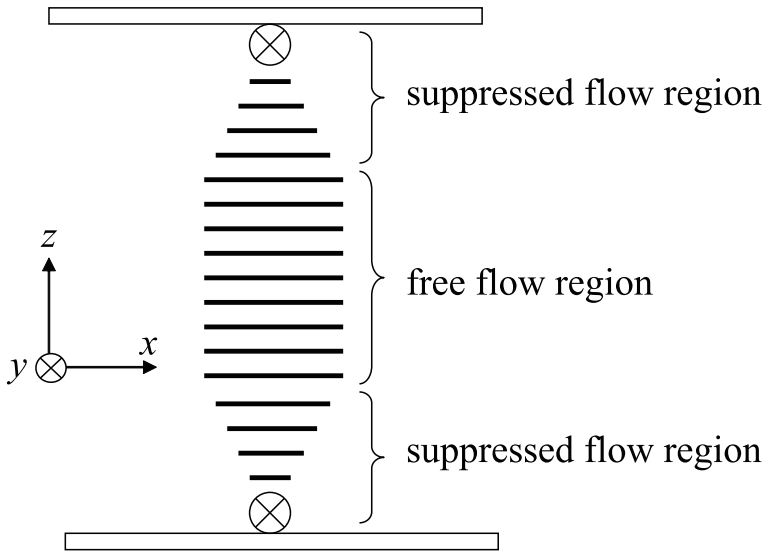

Figure 2.8. Schematic illustration of the director field on π-wall. The director field near two surfaces are twisted by the anchoring effect.

strength s. Namely, the flow mode is"symmetric" for the sign of s. For $s = -1/2$ disclination, the flow caused by the director rotation is opposite to the symmetric flow, resulting in negligible backflow. On the other hand, the two flow modes points the same direction around an $s = +1/2$ disclination. Moreover, the direction of the coupled flow is the same as that of the disclination movement. Because of this coupling, an $s = +1/2$ disclination is accelerated.

We consider the distribution of flow caused by the director rotation in order to explain the formation of suppressed and free flow regions, because the symmetric flow has no essential effect on the asymmetry in the annihilation dynamics. LC cells with $d \geq 2\mu$m is considered first. The director field between two glass plates is distributed as Fig. 2.8 on the so-called π-wall. The director near the cell surface is aligned by the anchoring effect. The angle between the director and the anchoring easy axis is smaller in comparison with that in the bulk region, whereas the anchoring effect is relatively small in the bulk region, where the director field is distributed as if there were no surfaces. In addition, the director field in the bulk region is mostly independent of the z coordinate.

After the disclination goes through, the angle between the director and the anchoring easy axis becomes zero. Considering the distribution of the director field, the director rotation near the surface is slower than that in the bulk region. Therefore the flow caused by the director rotation becomes weak near the cell surface. In the bulk region, the flow distributes uniformly. As for the symmetric flow, we assume that there is no specific cell gap as in the case of Poiseuille flow of isotropic fluids. The assumption is phenomenological, but does not have essential effect on the asymmetry in annihilation dynamics. Distributions of the two flow modes are schematically shown in Fig. 2.9. The total

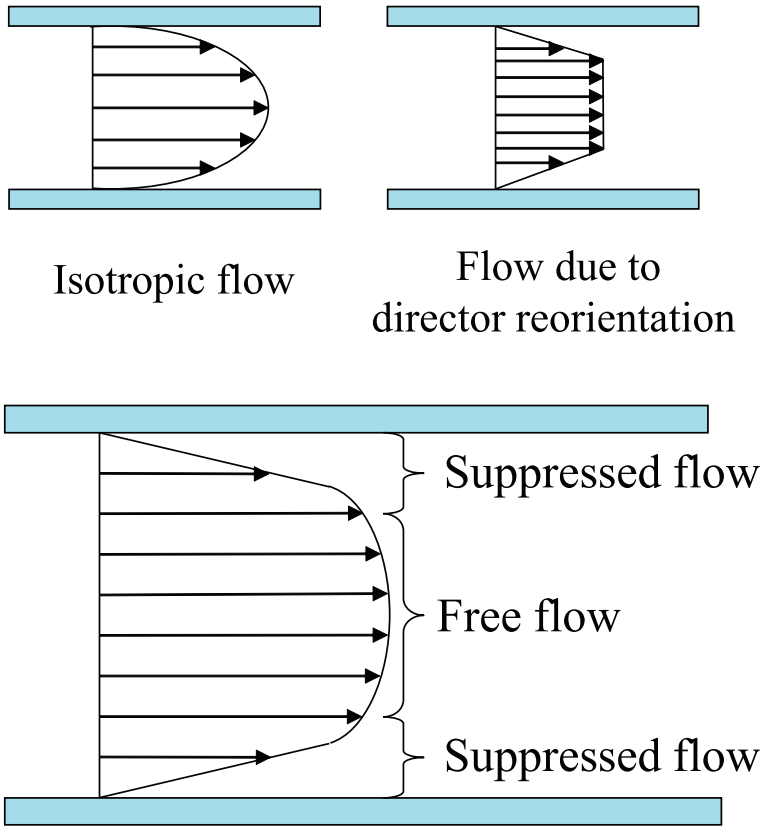

Figure 2.9. Distribution of flow coming from director rotation (a), symmetric flow (b), and total backflow around an $s = +1/2$ disclination (c).

backflow is a superposition of the two flow modes as shown in Fig. 2.9(c). It is expected that the total flow is almost independent of the z coordinates in the central part of the LC cell by virtue of the flat distribution of the director rotation flow. On the other hand, the backflow drops off rapidly as the cell surfaces come close. The gradual increase in v_+/v_- for $d \geq 2$ μm is explained by the increase in the maximum velocity of Poiseuille (symmetric) flow with increasing the cell gap d.

The suppression of the backflow in the LC cell with $d = 1$ μm is also explained on the basis of Fig. 2.9. Because of the small cell gap, the flat region in Fig. 2.9(a) is absent in the LC cell with $d = 1$ μm. Therefore all the thickness of LC cell belongs to the suppressed flow region. The velocity ratio v_+/v_- gets close to the unity.

To see the consistency of the above qualitative discussion with existing theories, we examine the director field around the π-wall. The angle between the director and the anchoring easy axis, denoted as φ , can be calculated on the basis of the elastic theory [12]. By putting the origin of coordinates on

a cell surface, the angle φ on the *yz*-plane (shown by a dashed line in Fig. 2.10(b)) is given by [12]

$$\varphi(y,z) = \frac{1}{2}\mathrm{Tan}^{-1}\left[\frac{2\sinh(\sqrt{\frac{K_2}{K_{sb}}}\frac{\pi}{d}y)\sin(\frac{\pi}{d}z)}{\sinh^2(\sqrt{\frac{K_2}{K_{sb}}}\frac{\pi}{d}y)-\sin^2(\frac{\pi}{d}z)}\right]. \tag{2.5}$$

Figure 2.10(a) shows the relation between φ and the distance from the lower surface for cell gaps used in the present study. The value of the *y* coordinate was set to the radius of disclination core ($r_c = 0.01$ μm) to fix the sense of director rotation ($\pm\pi/2$ is equivalent because of the head-to-tail symmetry of nematic phase). The angle starts at a small value on the cell surface ($z = 0$), increases rapidly without the dependence on the cell thickness d, saturates to $\pi/2$ (the surface-free value) if the cell is thick enough, and then return to the small value on the other surface ($z = d$). This is fully consistent with our expectation depicted in Fig. 2.8. In the LC cell with $d = 1$ μm, the maximum magnitude of φ is notably smaller than $\pi/2$. The suppression of the flow caused by the director rotation is expected throughout the cell.

2.5 Conclusion

We observed the annihilation dynamics of disclination pair under the strong anchoring condition. To see the backflow effect, we analyzed the ratio of velocities of $s = \pm 1/2$ disclinations. The ratio rapidly decreased when the cell gap d was reduced to 1 μm. It means that the backflow is suppressed in a thin LC cell. There is the suppressed flow region near the cell surface, where the effect of the surface anchoring is in effect. The angle between director and the anchoring easy axis at the surfaces is smaller in comparison with that in the central region of the LC cell. The director rotation involved in annihilation dynamics is slow near the cell surface, accordingly. Therefore the flow caused by the director rotation is significantly suppressed. When the cell gap d is 1 μm, the director rotation is suppressed throughout the whole thickness of the cell. This picture is supported by the calculated profile of the director field within an elastic theory.

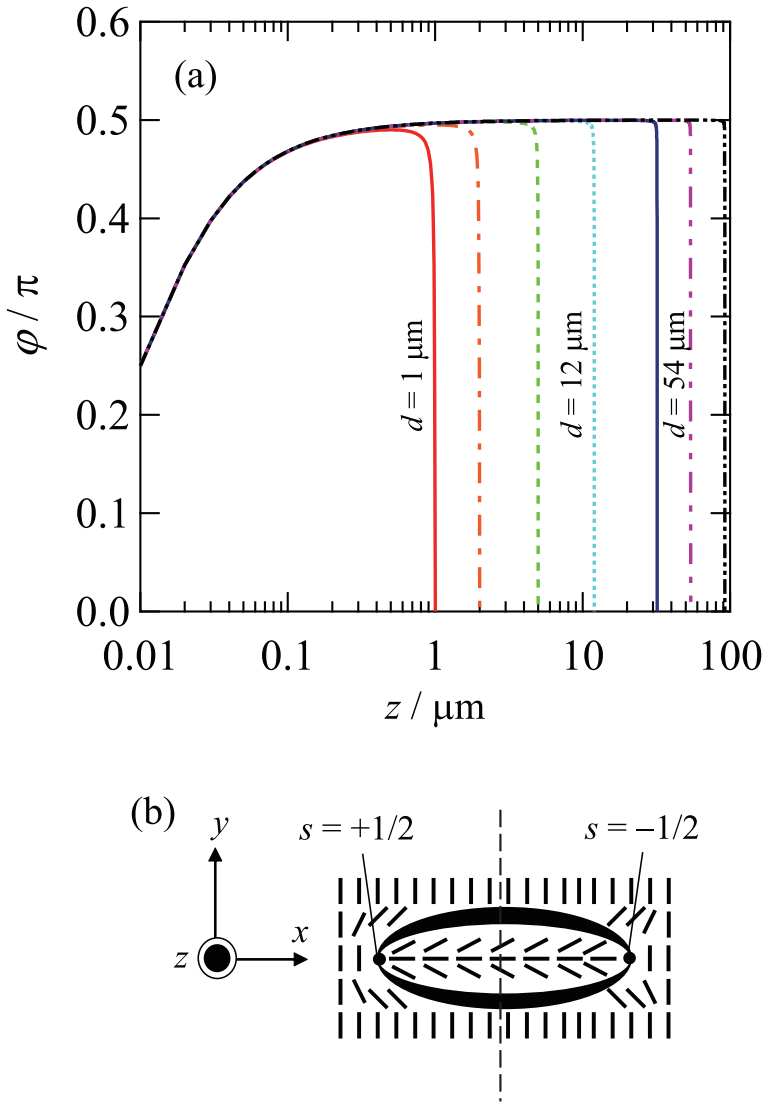

Figure 2.10. (a) Angle between y-axis and the director calculated by using Eq.2.5 for cell thicknesses d utilized in the present study. (b) Director field at $z = d/2$ with a disclination pair. The dashed line in (b) indicates the plane $x = 0$, where Eq.2.5 applies.

Chapter 3

Annihilation under external field and surface anchoring

3.1 Introduction

Surface anchoring effect on disclination dynamics and backflow was investigated in the previous chapter. Backflow is suppressed under the strong anchoring condition, and "suppressed flow region" is generated near the cell surface. It was revealed that the surface anchoring influences very thin region close to the surface. On the other hand, an external electric field deforms the whole region of the director field in the LC cell. Therefore the electric field can influence disclination motion in a more direct way. In this chapter, the effect of the external electric field is discussed, in addition to that of the strong anchoring.

Disclination dynamics under the external electric field has been discussed considering backflow. Blanc *et al.* [18] measured the electric-field-driven annihilation of nematic disclination pairs with $s = \pm 1/2$ in the nematic phase of 5CB. They used planarly oriented layers with a very weak azimuthal anchoring, thus enabling a free rotation of the director on the plane of the substrates. In a strong enough electric field, the anchoring becomes negligible. This simple experimental system allows a quantitative comparison with numerical studies based on the hydrodynamics of tensorial order parameter. The simulations showed that the asymmetry in the annihilation of the nematic disclinations is due to the backflow.

Backflow effect under the influence of cell surfaces has also been studied. Tóth *et al.* [23] studied the motion of disclination line that is parallel to the substrates. In this situation, backflow is confined between two cell surfaces. On the other hand, the backflow effect on annihilation dynamics under the strong anchoring condition remains totally unexplored.

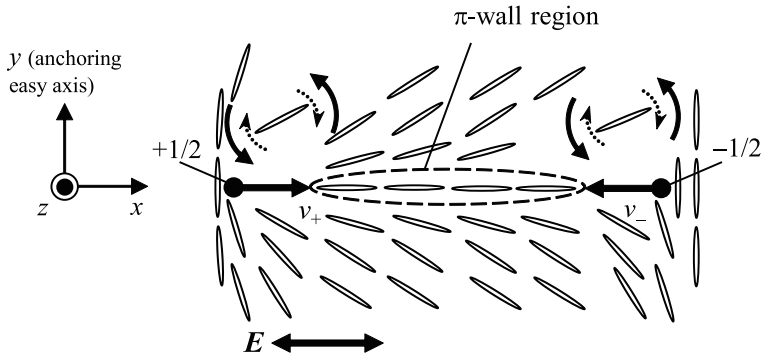

Figure 3.1. Configuration of the director around $\pm 1/2$ disclinations in the present experimental setup. The two dots are cores of these disclinations. These disclinations move parallel to the applied electric field. Curved arrows surrounding the director denote torques. The torque from the elastic energy (solid) is always opposite to that from the electric field (dotted).

In this chapter, presented is an experimental study of the dynamics of $\pm 1/2$ disclinations in the nematic phase of 5CB under the strong anchoring condition in an electric field. The results show that their motion is clearly asymmetric; The +1/2 disclination moves almost twice as fast as the $-1/2$ one even under the strong anchoring condition. This behavior essentially remains unchanged under electric fields up to 30 V/mm. The backflow effect under the electric field is discussed.

3.2 Experimental

Nematic phase of 5CB was selected as a sample to study the disclination dynamics. 5CB was sandwiched between two glass plates coated with a homogeneous alignment material. Poly(vinyl alcohol) (PVA) solution (1% in concentration) was used as the homogeneous alignment material. Details of the surface treatment process was shown in Chapter. 2.

Aluminum foil (12 μm in thickness) was used as spacers and electrodes to apply a dc electric field parallel to the glass plates. Each electrode was 0.3 mm in width and 10 mm in length. Two electrodes were arranged parallel to the easy axis of anchoring at an interval of 0.5 mm. An electric fields was applied perpendicularly to the easy axis, to which the two glass plates were parallel.

Disclinations in nematic phase were generated by quenching the sample from the isotropic phase ($T = 36.0$ °C) to the nematic phase (34.8 °C), and then the sample temperature was kept constant within ± 0.1 °C by using a hot stage for observation. The experimental configuration is schematically shown in Fig. 3.1.

Images of disclination pairs were recorded through a CCD camera mounted on a polarizing micro-

scope. After the sample was quenched, the dynamics of the disclination pair moving perpendicularly to the anchoring easy axis was observed. The applied dc electric field ranged from 0 to $\pm$30 V/mm.

3.3 Results

A typical time dependence of the distance u between a disclination pair is shown in Fig. 3.2. When the disclination pair is largely separated, u decreases linearly with time. On the other hand, there is a slight deviation downward from the extrapolation line with a constant speed shortly before the annihilation of the disclinations. Although the relative velocity of the disclination pair gradually decreases with increasing electric field, the time dependence of u is essentially the same as that at the zero electric field. This behavior is simply explained in terms of an elastic model proposed by Bogi *et al.* [12], where the anchoring energy is taken into account. According to them, during the time course, u satisfies the following equation

$$v_{\mathrm{asy}}t = u_0 - u + \xi_{\mathrm{c}} \ln\left(\frac{u+\xi_{\mathrm{c}}}{u_0+\xi_{\mathrm{c}}}\right), \tag{3.1}$$

where u_0 is the initial distance between the disclinations. v_{asy} is the initial annihilation speed given by

$$v_{\mathrm{asy}} = \frac{16\sqrt{K_{\mathrm{sb}}K_2}\left[\frac{\pi}{2} - 1 + C + \frac{\pi}{2}\ln\left(\frac{d}{\pi L}\right)\right]}{d\pi\gamma_{\mathrm{eff}}\ln\left(\frac{3.6\xi_{\mathrm{c}}}{r_{\mathrm{c}}}\right)}. \tag{3.2}$$

In Eq. 3.1, ξ_{c} is a characteristic length, which represents the radius of a cylinder around each defect where the elastic torque associated with the defects dominates the anchoring torque. In the region $u \gg \xi_{\mathrm{c}}$, the direct elastic interaction between disclinations is completely screened out by the anchoring energy. The disclinations approach each other with a constant speed v_{asy} (stationary regime), accordingly. On the other hand, in the region $u < \xi_{\mathrm{c}}$, the elastic interaction of two anchoring-free disclinations is in effect. The distance between disclinations follows a square-root time law (accelerating regime). Thus, a crossover between the stationary and accelerating regimes occurs at approximately $u \approx \xi_{\mathrm{c}}$. Since the square-root time law was observed only just before the annihilation of disclinations in the present study, the time dependence of u is described by Eq. 3.1 with $\xi_{\mathrm{c}} \to 0$. This means that the direct elastic interaction between disclinations plays only a minor role in the disclination dynamics, and therefore the present cell successfully provides a strong anchoring condition.

Figure 3.3 shows the position of two annihilating disclinations with $s = +1/2$ (upper side) and $s = -1/2$ (lower side), as a function of time. Here, we define x as the axis connecting the two

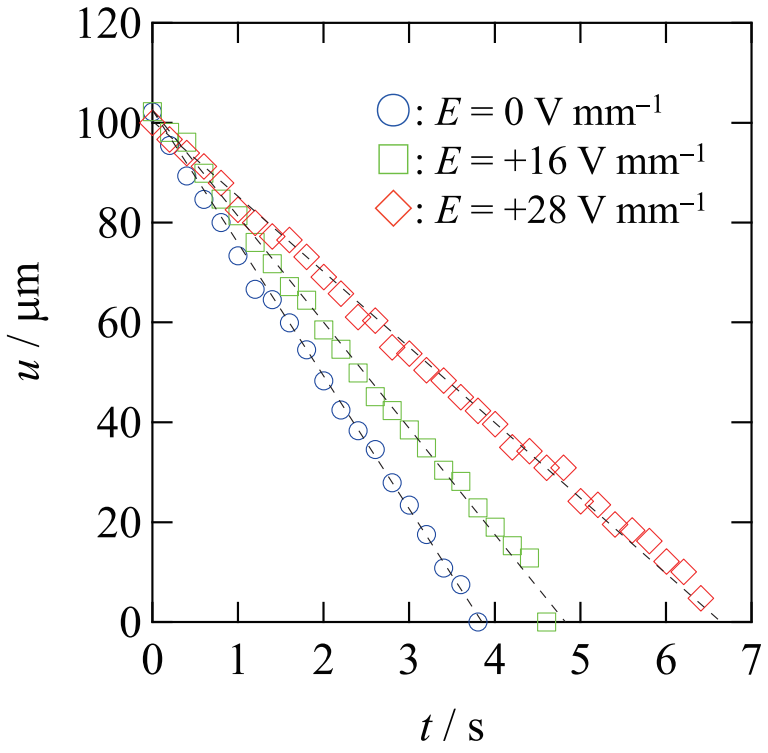

Figure 3.2. Time dependence of the distance u between a disclination pair in dc electric fields of 0, 16, and 28 V/mm. There is a slight deviation downward from the straight line (dashed, with a constant speed) shortly before the annihilation of the disclinations.

disclination cores (see Fig. 3.1). Asymmetric motion with +1/2 defects moving faster than $-1/2$ defects is clearly seen by inspecting the meeting point, which is not the midpoint between the initial positions of the defects. A similar asymmetry in the defect motions was also observed in the case of applied electric fields. Note that the $s = \pm 1/2$ disclinations exhibit stationary velocities most of the time.

Now, we focus on the stationary dynamics of the pair of disclinations. Figure 3.4 shows the electric field dependences of v_+ and v_-, where v_+ (v_-) is the stationary velocity of the disclination with s = +1/2 ($-1/2$). For comparison, $v_{\rm asy}$ ($= v_+ + v_-$) is also shown. v_+, v_-, and $v_{\rm asy}$ decrease gradually with increasing electric field. Similar results were obtained when the direction of the electric field was reversed (not shown).

To discuss the role of the backflow, we quantify the symmetry-broken dynamics using the ratio of v_+/v_-. Figure 3.5(a) shows the ratio v_+/v_- as a function of electric field. v_+/v_- is almost independent of the electric field up to 30 V/mm with a constant value of ~ 1.6, which is slightly smaller than that in a weak anchoring case [16–18, 23, 27]. Since the $s = -1/2$ disclination is only slightly affected by the backflow, v_- can be regarded as the velocity of the defect without the backflow effect. Figure

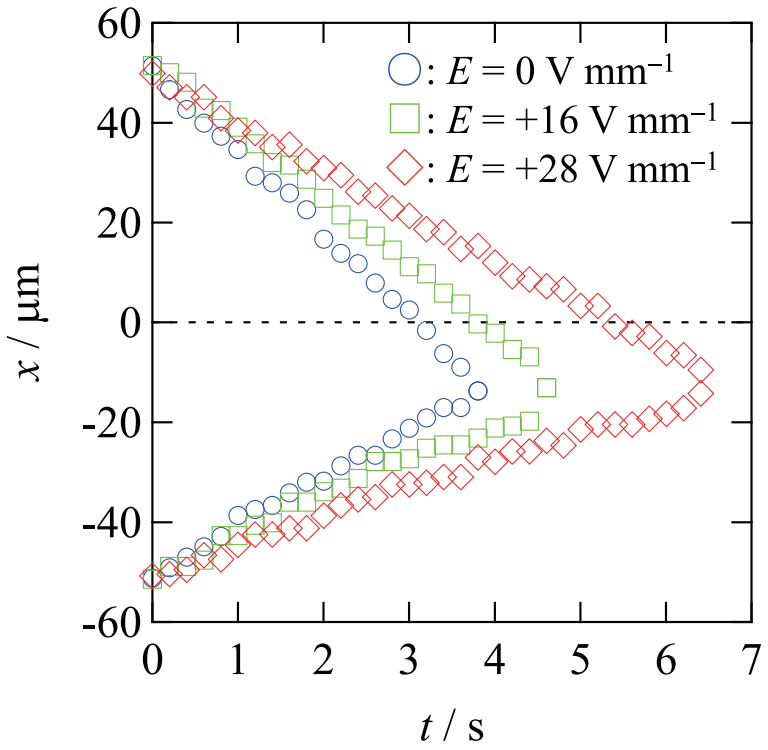

Figure 3.3. Motion of the disclinations towards their annihilation in electric fields of 0, 16, and 28 V/mm. The x-axis is defined as the axis connecting the two annihilating disclinations. The position of the $s = +1/2$ $(-1/2)$ disclination is positive (negative) at $t = 0$.

3.5(b) shows v_+/v_- as a function of v_-. We notice that v_+/v_- is also independent of v_-. Our results show that s = +1/2 disclinations systematically move faster than $s = -1/2$ ones.

3.4 Discussion

Let us discuss the effect of an electric field on the annihilation under a strong anchoring condition. The velocities of $\pm 1/2$ disclinations decrease with increasing the electric field. The reduction in disclination speed should be explained by a mechanism that does not affect the growth of backflow. Possible origins of disclination speed reduction are as follows: (i) electrohydrodynamic convection (EHC) of the NLC, (ii) a change in the viscosity of 5CB with electric field application, and (iii) a change of elastic energy of 5CB with electric field application.

The characteristic pattern of EHC [28–30] was not observed in the present experiments. Therefore EHC is not the cause of the velocity reduction. The change in viscosity is also not the cause of the velocity reduction, because the reduction in velocity is too large to be explained by the change in viscosity [31]. Furthermore, hypotheses (i) and (ii) would change the velocity ratio. Consequently,

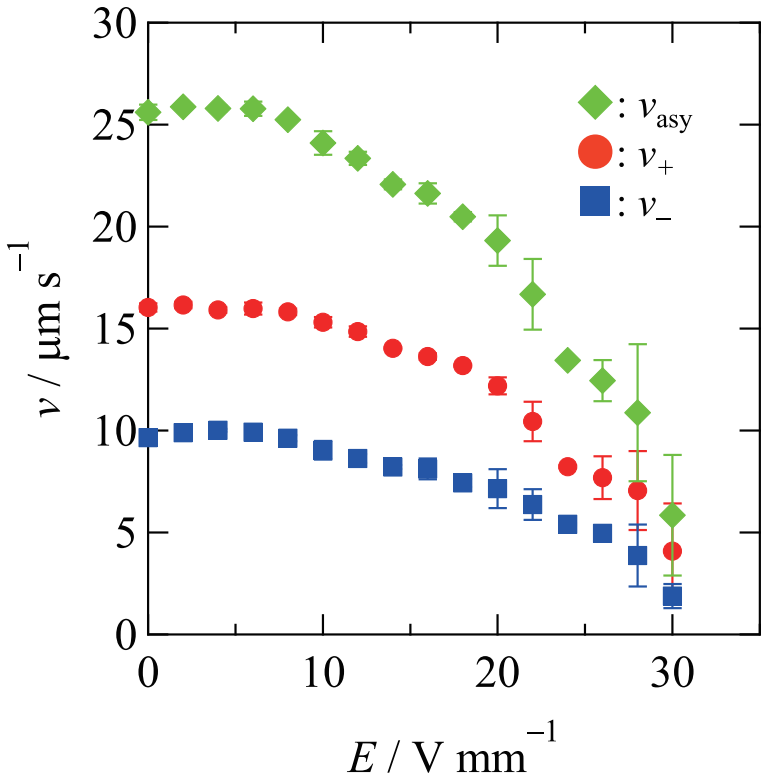

Figure 3.4. Electric field dependences of v_+, v_- and v_{asy}.

these hypotheses are discarded.

The reduction in disclination speed can be qualitatively understood by considering a change in elastic energy due to an applied electric field [hypothesis (iii)]. It is known that the coupling term in free energy between a dc electric field and the director field has the form [1],

$$f_{el} = -\frac{1}{2}\varepsilon_0\varepsilon_a E^2 \cos^2\theta, \tag{3.3}$$

where ε_a is the dielectric anisotropy (positive for 5CB), and θ the angle between the director and the electric field. In our experimental configuration shown in Fig. 3.1, the director in the bulk region is perpendicular to the electric field ($\theta = \pi/2$) owing to the strong anchoring, while that on the π-wall is parallel to the electric field ($\theta = 0$). Considering the positive dielectric anisotropy of 5CB, the π-wall region is stabilized by $\varepsilon_0\varepsilon_a E^2/2$ compared with the bulk region. The energy per unit length of the π-wall is equal to the constant driving force, which dominates the velocity of the disclination in the region $u \gg \xi_c$ [12, 18]. Hence the driving force of annihilation is weakened under an electric field, resulting in the reduced velocity of the disclination. The disclination velocities v_{asy}, v_+ and v_- are in proportion to elastic energy. The observed decrease in Fig. 3.4 is roughly quadratic as expected from Eq. 3.3.

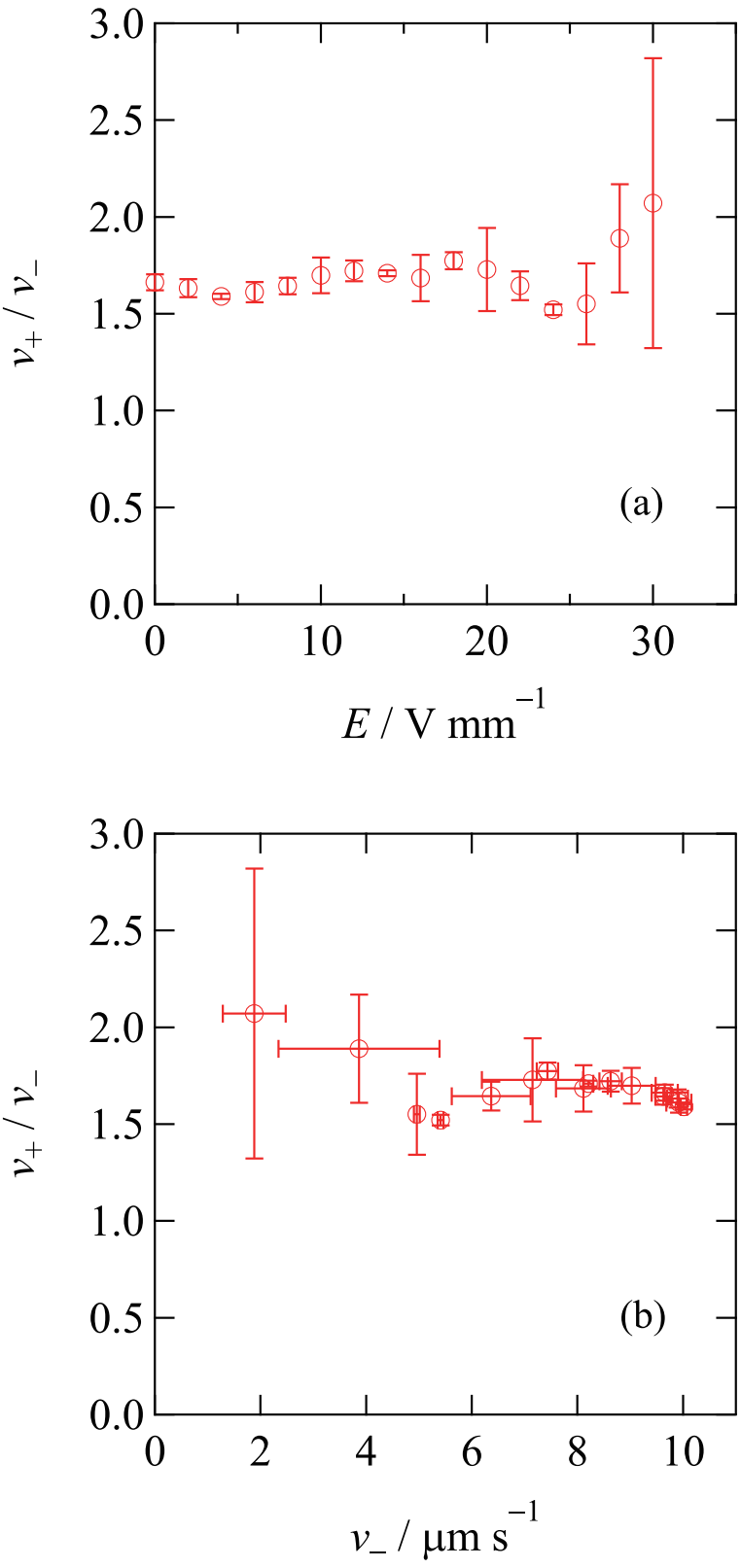

Figure 3.5. Ratio v_+/v_- as a function of electric field (a) and v_- (b).

The discussion on the stabilization of the π-wall given above does not consider how two disclinations approach each other while accompanied by the deformation of the director filed. The velocity of disclinations is also influenced by the suppression of the director rotation around disclinations. The director field around disclinations is different from that in the exact (and idealized) π-wall region (plane). The director near disclinations is in rotary motion owing to the disclination dynamics. We have to consider the balance of three types of torque arising from the elastic energy, the electric field, and the viscosity. The torque from viscosity arises only to balance the sum of the elastic and dielectric torques in the case of the stationary dynamics considered in this study. This is true even under a strong anchoring condition. We discuss the elastic and dielectric torque in order to explain the disclination motion under a strong anchoring and an electric field. The director field near $\pm 1/2$ disclinations in the middle of the cell in its thickness direction is shown in Fig. 3.1. Under a strong anchoring condition, the director near the cell surfaces is parallel to the anchoring easy axis. Along the cell thickness (z-axis), therefore, the angle between the director and x-axis changes from 0 to $\pi/2$ (maximum). Because of this twist, the director is subjected to a torque, the sense of which depends on the side of the π-wall. This torque arising from the twist deformation is shown as solid curved arrows in Fig. 3.1 Since the director at the surface is fixed by a strong anchoring, the torque forces the director to rotate toward the anchoring easy axis. On the other hand, the electric field forces the director to be parallel to the π-wall. Considering again the positive dielectric anisotropy of 5CB, the dielectric energy becomes minimum when the director is parallel to the π-wall. This dielectric torque is shown in Fig. 3.1 by dotted arrows. The dielectric torque has the opposite sense to the elastic torque. Thus, the rotation of the director is suppressed by an external electric field. The external electric field makes the rotational relaxation around disclintions slower by this mechanism. For disclinations to be stationary, the torques arising from twist elasticity, electric anisotropy and viscosity must be closely balanced. Since the torque from the dielectric anisotropy is always opposite the rotation necessary for the movement of disclinations, the sum of the elastic and dielectric torques, i.e., the total driving force, becomes smaller. The torque from viscosity is a function of director rotation speed. A smaller driving force generates the slower director rotation, and the torque from viscosity becomes smaller, accordingly. It is emphasized that our model is for a time course when directors are just rotating associated with the movement of disclinations. This model of torque balance is valid under a strong anchoring condition and a smaller electric field than the cutoff of the Frederiks transition (estimated as *ca.* 35 V/mm for the present experimental setting).

Finally, a comment is given on the reason why the ratio of defect velocities remains constant under external electric fields. Figure 3.1 shows that the mechanism for the slowing down applies regardless

of the sign of $s = \pm 1/2$ disclinations. The suppression of director rotation around the $s = \pm 1/2$ disclination is explained by the elastic (i.e., stationary) theory. Since there is no plausible reason to assume that hydrodynamic parameters are altered by the external electric field, the backflow arises in the same way as under the zero electric field condition, and the ratio of disclination velocity remains constant.

3.5 Conclusion

We have presented an experimental study of the dynamics of disclinations with $s = \pm 1/2$ in a NLC under a strong anchoring condition in an electric field. v_+/v_- is almost independent of the electric field up to 30 V/mm with a constant value of ~ 1.6, which is slightly smaller than that in a weak anchoring case. Moreover, v_+/v_- is independent of v_-, which can be regarded as the velocity of defects without the backflow effect. Our results show that $s = +1/2$ disclinations systematically move faster than $s = -1/2$ ones. The backflow effect under a strong anchoring condition is very similar to that without the anchoring effect. These experimental results suggest that a strong velocity vortex pair is formed around the $+1/2$ defect even under a strong anchoring condition. An electric field significantly affected the rotation of director around disclinations, but only slightly affected the occurrence of backflow near $s = \pm 1/2$ disclinations.

Chapter 4

Ultraslow oscillation of disclination after abrupt switching of voltage

4.1 Introduction

In Chapter 2 and 3, the annihilation dynamics of the nematic disclinations was investigated under the stationary external forces. The annihilation dynamics was reasonably analyzed based on the continuum theory of the NLC. In previous chapters, disclination dynamics was analyzed based on the assumption that the external force balance the viscous drag. In this sense, the motion of a disclination in a quasi-steady state has been studied so far.

If the deformation of the director field is large and time-dependent, the deformation will also depend on the position and velocity of the disclination. In particular, when an electric field is applied to a liquid crystal (LC), such deformation is easily introduced. Since the force acting on the disclination also depends on time (and position), the disclination dynamics will become more complicated.

Disclination dynamics under a high-frequency ac field has been well discussed. [18] Because the dielectric energy of an LC is proportional to the square of the field strength, the effect of a high-frequency ac field can be regarded as identical to that of a dc field. Actually, the annihilation dynamics of a disclination pair under a dc field was reported to be the same as that under a steady ac field. [32] The frequency used in past studies was, however, higher than the relaxation frequency of the director field but lower than the relaxation frequency of dielectric dispersion due to molecular reorientation. [33] It is possible that dc and ac voltages may exert different effects on the disclination dynamics accordingly. Since the quasi-stationary dynamics has been successfully analyzed assuming the equivalence of dc and ac fields, such a difference might appear in the dynamics immediately after applying dc and ac voltages.

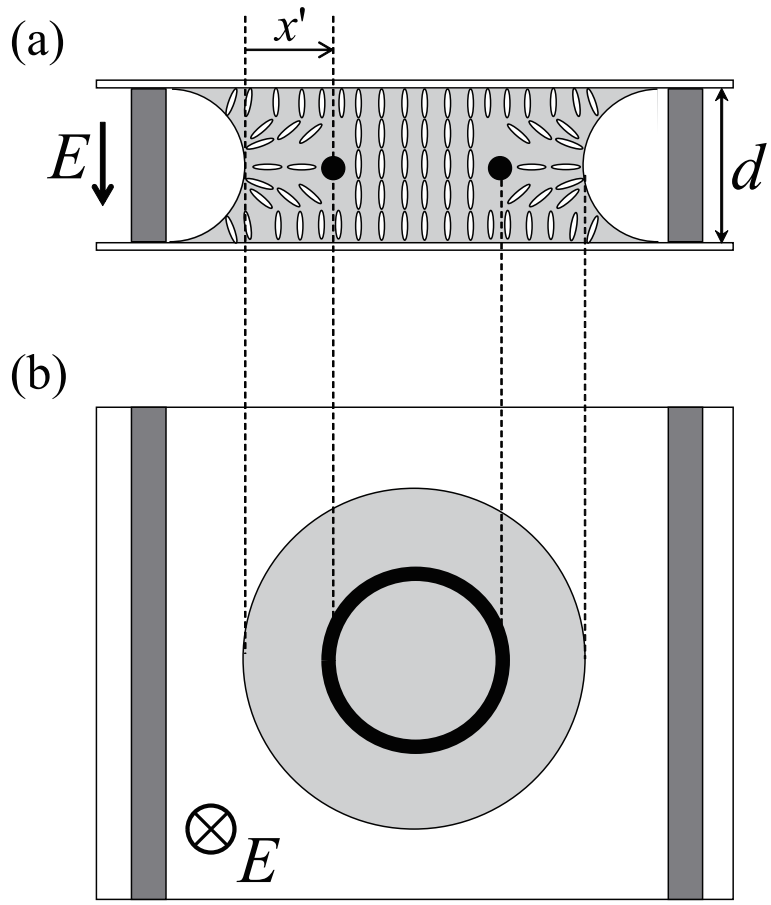

Figure 4.1. Schematic illustrations of LC cell. Cross-sectional view (a) and top view (b). In (a), the director field is also shown schematically.

In this chapter, we performed experiments to record the relaxation dynamics of an isolated nematic disclination bound to an air-LC interface by applying an abrupt (stepwise) change in the electric field. The damped oscillation of the disclination with a very long time scale was observed after switching only under the dc voltage. The details of the oscillation (amplitude and cycle) depend on the history of voltage switching.

4.2 Experimental

It is known [34] that an isolated and stable disclination ($s = -\frac{1}{2}$) ring is formed at its periphery when a droplet of nematic LC is sandwiched between two planar substrates having preferential perpendicular alignment, as schematically shown in Fig. 4.1. The surface facing the air forms a meniscus, to which the local director field is perpendicular at all points. Then, a disclination line is introduced along the interface.

8CB (nematic-isotropic phase transition temperature T_{NI} = 40.5 °C) was selected as a nematic

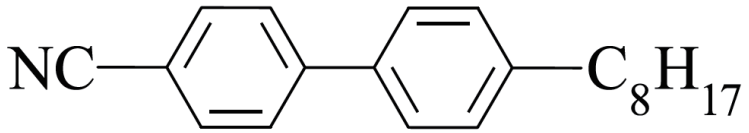

Figure 4.2. Molecular structure of 8CB.

LC sample because its material parameters are well known. [35–38] A schematic view of our experimental system is shown in Fig. 4.1. An 8CB droplet was sandwiched between two indium tin oxide (ITO)-coated glass plates. The glass surface was treated with a vertical alignment material [*n*-octyltriethoxysilane (Z-6341)]. Since the director is aligned perpendicular to the surface of the substrates and the air-LC interface, a disclination ring was stably introduced near the air-LC interface. The cell gap d was controlled by a spacer made of polyimide tape. The thickness of the cell and glass plates was measured five times, and the arithmetic mean of 55 μm was adopted as d. The temperature ($T = 39.0\,^{\circ}$C) was kept constant within $\pm 0.1\,^{\circ}$C using a hot stage and a temperature controller (INSTEC HCS302 and mK1000). The temperature was monitored by using a thermocouple placed near the sample. Images of the disclination were recorded using a digital camera with spatial and time resolutions of 0.19 μm/pixel and 30 frames/s, respectively.

The disclination dynamics was observed by exerting an abrupt (stepwise) change in the applied voltage to the cell. In the dc experiments, the pair of applied dc voltages was changed systematically as follows. First, the initial voltage $V_{\rm i}$ was set to -1.00, 0.00, 0.50, 1.00, 1.50, and 3.00 V while keeping the final voltage at $V_{\rm f}$ = 2.25 V. Second, $V_{\rm f}$ was varied from 1.75 to 2.50 V with $V_{\rm i} = 0.00$ V. Third, both $V_{\rm i}$ and $V_{\rm f}$ were changed while their difference was kept at $V_{\rm f} - V_{\rm i} = 1.25$ V. In the ac experiment for comparison, $V_{\rm f} = 2.00$ V (RMS value, 1 kHz) and $V_{\rm i} = 0.00$ V were used.

4.3 Results

The trajectory of the disclination was obtained by analyzing movies of its motion. The recorded movies were converted to a set of luminance (greyscale) data. In order to reduce the noise in the luminance data, the luminance was averaged out in each frame along the disclination line (150 pixels in length), which is short enough to ignore the curvature of the disclination. Considering that the luminance reaches a minimum at the disclination position, the integrated luminance data for each frame were fitted to a Gaussian to locate the disclination position as the minimum point of the fitted

curve. The disclination position x' was measured from the air interface.

The general behavior of the motion of a disclination observed under a dc voltage is as follows. A disclination remains stationary under a voltage of V_i before the change in voltage. When the voltage is switched to V_f at $t = 0$, the disclination starts to move toward to the equilibrium position x_0. After some relaxational (oscillatory) motion around the equilibrium position, the disclination stops. The air-LC interface did not move upon switching the applied voltage. The displacement of the disclination is written as $x = x' - x_0$. The trajectories of the disclination are shown in Fig. 4.3.

Note that the existence of the equilibrium position x_0 is essential for a relaxation resembling a damped oscillation. The existence arises from the balance between the dielectric force and the repulsive force from the air-LC interface. Such relaxation would only be observed for a bound disclination at an air-LC interface.

In Fig. 4.3(a), trajectories with the same V_f are shown. The amplitude of oscillation and the velocity of the disclination increases with decreasing V_i. With $V_\mathrm{i} = 3.00$ V ($> V_\mathrm{f} = 2.25$ V), the sense of the oscillation is reversed because the starting point of the disclination is on the opposite side of the equilibrium position. When the difference between the start and final voltages is kept constant [1.25 V, Fig. 4.3(b)], the maximum amplitude of the oscillation decreases with increasing V_f. This is explained by considering the fact that the distance between the disclination and the air interface is larger for a smaller voltage because of the shift of the equilibrium position (x_0) as shown in Fig. 4.3(b). If the repulsive force acting on the disclination strongly depends on the distance from the air interface, the disclination moves more easily under a weak voltage, giving a damped oscillation with a large amplitude.

The trajectory under an ac voltage is shown in Fig. 4.4. The disclination monotonically approaches the equilibrium position and ceases to move within 20 s. Namely, the disclination relaxes much faster under an ac voltage than under a dc voltage. This implies that the director field relaxes faster under an ac voltage than under a dc voltage. The elastic energy causes a minimum within a short time under an ac voltage accordingly. Figures 4.3 and 4.4 imply that the detailed behavior of the relaxation depends on the frequency of the applied voltage. Since the dielectric energy of an LC is theoretically proportional to the square of the field strength, dc and ac fields have indistinguishable effects if the frequency of the ac field is high enough. In the present experiment, the frequency is high enough relative to the motion of the disclination, as evidenced by the nonsynchronous motion under the applied voltage. However, the experimental results show that the disclination dynamics under an ac voltage is different from that under a dc voltage.

Since the diameter of the droplet is large enough (≈ 5 mm) compared with the amplitude of

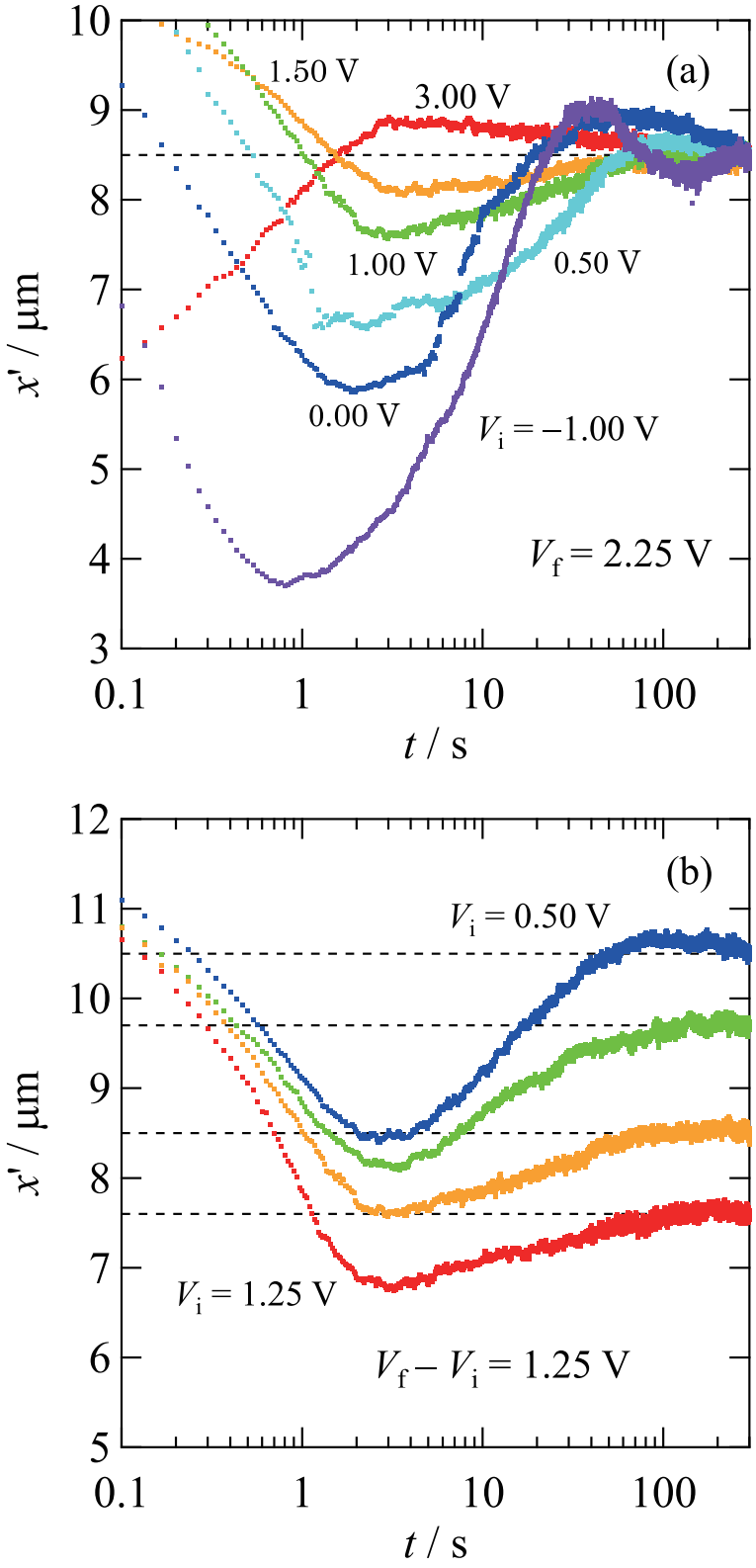

Figure 4.3. Damped oscillation of a disclination (a) under a constant final voltage ($V_f = 2.25$ V, $V_i = -1.00$, 0.00, 0.50, 1.00, 1.50, 3.00 V) and (b) driven by a constant $\Delta V = V_f - V_i$ ($V_i = 0.50$, 0.75, 1.00, 1.25 V and $\Delta V = 1.25$ V).

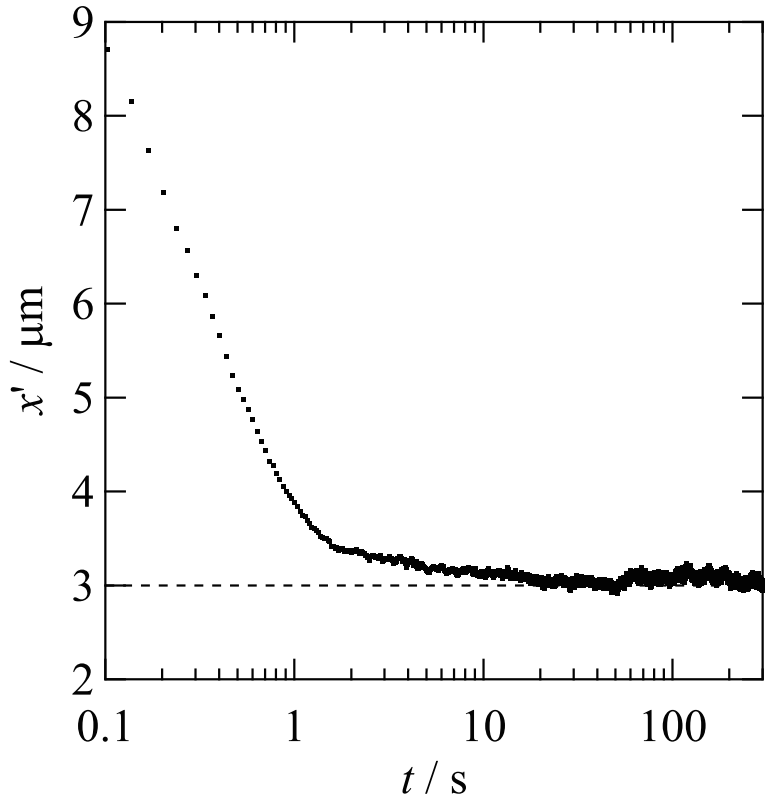

Figure 4.4. Disclination dynamics under an ac voltage ($V_{\rm i} = 0.00$ V, $V_{\rm f,RMS} = 2.00$ V, 1 kHz).

oscillation (≤ 5 μm), the disclination can be regarded as a straight line. Consequently, little effect of the line tension of the disclination is expected for its oscillatory motion normal to the line. The effect of backflow is also ignored here because it is known that the backflow around an $s = -1/2$ disclination is very weak under an external voltage [23]. In more advanced studies, needless to say, the flow dynamics of LC is taken into account [39].

In order to experimentally extract the characteristics of the observed dynamics, we examine the value of $(\tau/2)_{\rm app}$ (the time difference between successive crossings at the equilibrium position x_0) under a constant $V_{\rm f}$. Figure 4.5 is a plot of $(\tau/2)_{\rm app}$ with $V_{\rm f} = 2.25$ V as a function of $x_{\rm ex}$, at which the trajectory exhibits an extremum between the nodes defining $(\tau/2)_{\rm app}$. It is evident that $(\tau/2)_{\rm app}$ increases when $x_{\rm ex}$ is closer to 0. That is, the oscillation becomes slower over time. This implies that the force field acting on the disclination is highly anharmonic with a negligible linear term.

Figure 4.5 implies that a nonlinear force field acts on the disclination. The driving force depends on the disclination position, x. The force can be roughly estimated through the analysis of disclination velocity, assuming that it balances with the viscous drag. Based on the assumption, the driving force

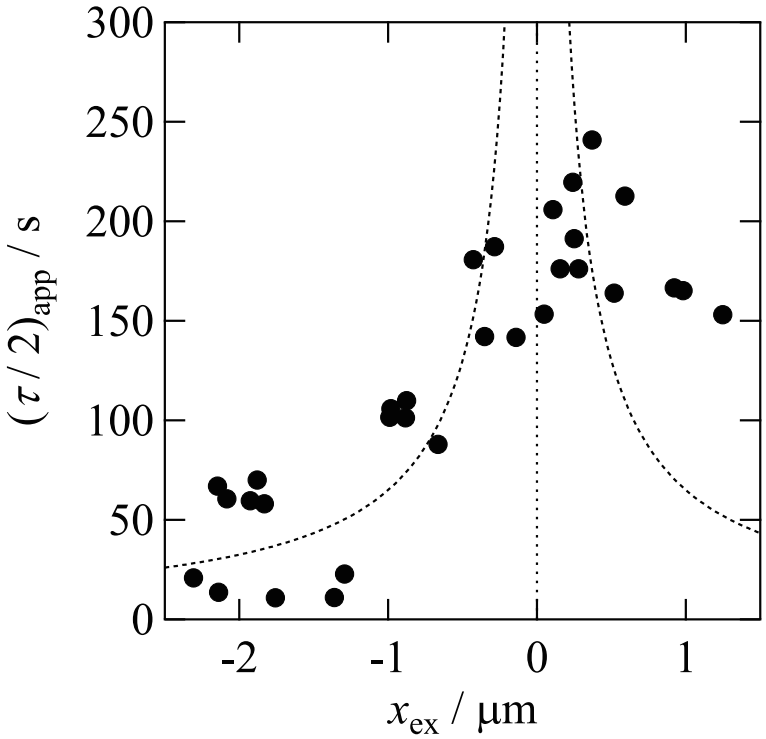

Figure 4.5. $(\tau/2)_{\mathrm{app}}$ (time difference between successive crossings) as a function of x_{ex} (positions of extrema of trajectory) under $V_{\mathrm{f}} = 2.25$ V. The broken line represents the half period of a harmonic oscillator having an effective force constant $k_{\mathrm{eff}} = \frac{1}{2}kx_{\mathrm{ex}}^2$.

acting on the disclination is given as follows.

$$G_0 - \Gamma v = 0,$$
$$G_0 = \Gamma v. \tag{4.1}$$

An estimate of the disclination velocity is thus given by

$$v = \frac{dx}{dt} \approx \frac{x_{\mathrm{ex}}}{\Delta t}. \tag{4.2}$$

Here Δt is a time, during which the disclination moves from the extrema to the equilibrium position, and Γ the relevant viscosity.

The viscosity Γ has been theoretically given as [10, 11]

$$\Gamma_{\mathrm{theor}} = \frac{\pi}{4}\gamma_{\mathrm{eff}} \ln \frac{\xi_{\mathrm{E}}}{r_{\mathrm{c}}}, \tag{4.3}$$

but it was later experimentally revealed that $\Gamma = \frac{1}{2}\Gamma_{\mathrm{theor}}$ is a better estimate. [40, 41] ξ_{E} is an electric coherence length written as

$$\xi_{\mathrm{E}} = \frac{1}{E}\sqrt{\frac{K_1}{\varepsilon_0 \varepsilon_{\mathrm{a}}}}. \tag{4.4}$$

Elastic constant K_1 is set to be K_1 = 4.48 pN, and $\gamma_{\mathrm{eff}} = 0.0289$ Pa s. Using material parameters for 8CB [10, 35, 36] and setting a core radius of the disclination of $r_{\mathrm{c}} = 100$ Å, [12] a numerical estimate yields $\Gamma = 0.077 - 0.073$ Pa s ($1.75 - 2.50$ V).

The driving force G_0 estimated based on Eq. 4.1 is plotted against x_{ex} in Fig. 4.6. All of experimental results are shown in Fig. 4.6. For $V_{\mathrm{f}} - V_{\mathrm{i}} \geq 2.25$ V, G_0's are scattered, and it is hard to identify any tendency, accordingly. On the other hand, G_0 systematically decreases with increasing x_{ex}, for $V_{\mathrm{f}} - V_{\mathrm{i}} < 2.25$ V. It changes mildly around equilibrium position, and it increase rapidly when disclination approaches the air-LC interface. Namely, the dependence of G_0 on x_{ex} is nonlinear. Since the director field between the disclination and the air-LC interface is deformed in their close approach, the elastic energy increases and repulsive force acts on the disclination. The increase of G_0 is thus qualitatively explained by the elastic theory.

Neither the microscopic (molecular) nor the mesoscopic (elastic) mechanism of the disclination dynamics can be plausibly imagined at present. We therefore consider a phenomenological model while regarding the disclination as a massive object. By doing so, the observed behavior can be described in a simple way. The disappearance of the oscillation under an ac voltage may be described

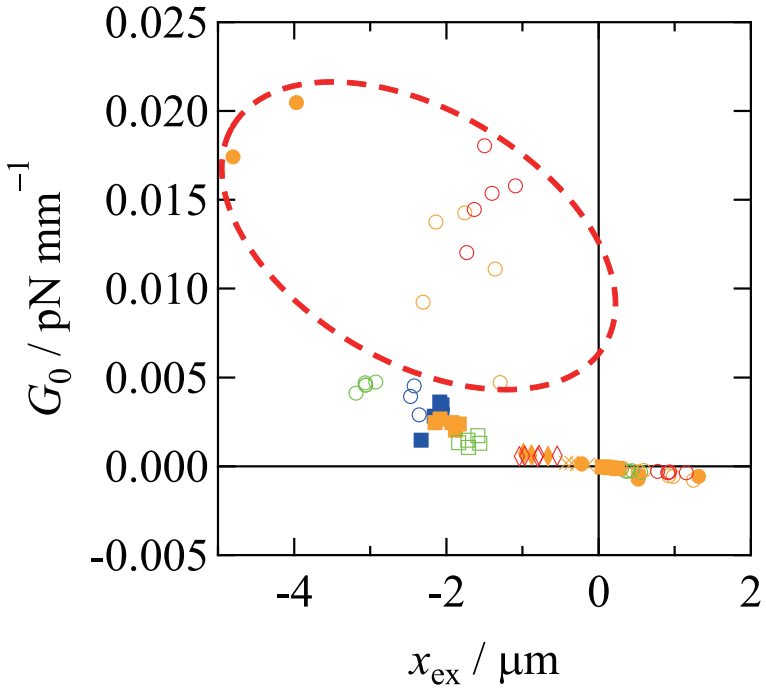

Figure 4.6. Relation between estimated driving force G_0 and x_{ex}. Dashed circle shows the results with $V_f - V_i$ larger than 2.25 V. Applied voltages are represented as (V_i, V_f). +, (3.00 V, 2.25 V); ×, (1.50 V, 2.25 V); ♦, (1.00 V, 2.25 V); ■, (0.50 V, 2.25 V); ●, (−1.00 V, 2.25 V); ◊, (1.25 V, 2.50 V); □, (0.75 V, 2.00 V); ■, (0.50 V, 1.75 V); ○, (0.00 V, 2.50 V); ○, (0.00 V, 2.25 V); ○, (0.00 V, 2.00 V); ○, (0.00 V, 1.75 V).

as a kind of overdamping in this model. The following equation of motion is assumed as the starting point:

$$\rho \frac{d^2x}{dt^2} = G(x) - \Gamma \frac{dx}{dt}. \tag{4.5}$$

Here, ρ is the effective mass a unit length, Γ is the relevant viscosity, and $G(x)$ is the elastic force field acting on the disclination. If $G(x)$ is a linear function of x, the right-hand-side of Eq. (4.5) becomes one for a simple damped oscillator with a harmonic spring.

The force field relevant to the observed slow dynamics of the disclination starts from a cubic term of x accordingly. The force field is approximately written as $G(x) = -kx^3$. This formula also crudely explains the behavior of $(\tau/2)_{\mathrm{app}}$. Assuming that the potential energies at x_{ex} are equal to each other for a real (anharmonic) disclination and a virtual harmonic oscillator having an effective force constant k_{eff}, i.e., $\frac{1}{2}k_{\mathrm{eff}}x_{\mathrm{ex}}^2 = \frac{1}{4}kx_{\mathrm{ex}}^4$, then the half period of the harmonic oscillator $(\tau/2)$ is expected to satisfy $\tau/2 \propto 1/|x_{\mathrm{ex}}|$. This seems consistent with the experimental results as shown in Fig. 4.5.

Assuming an elastic driving force of the form $G(x) = -kx^3$, the constant k was deduced from each experimental trajectory shown in Fig. 4.3. The time dependence of x around an inflection point was fitted to a cubic polynomial to obtain the position and velocity of the disclination at the inflection point. These two quantities suffice to fix k because the acceleration is zero at an inflection point. Using Γ and k thus determined, Eq. (4.5) was numerically integrated by the Runge-Kutta method (an example is shown in the inset of Fig. 4.8) with various ρ. Each calculation was started from the time when x is at the minimum with null velocity, because some other phenomena such as the relaxation of the elastic field, in principle, occur immediately after the change in the applied electric field. For example, the director field relaxes within 0.7 s. The time when x passes through the inflection point was treated as the "fitting" criterion.

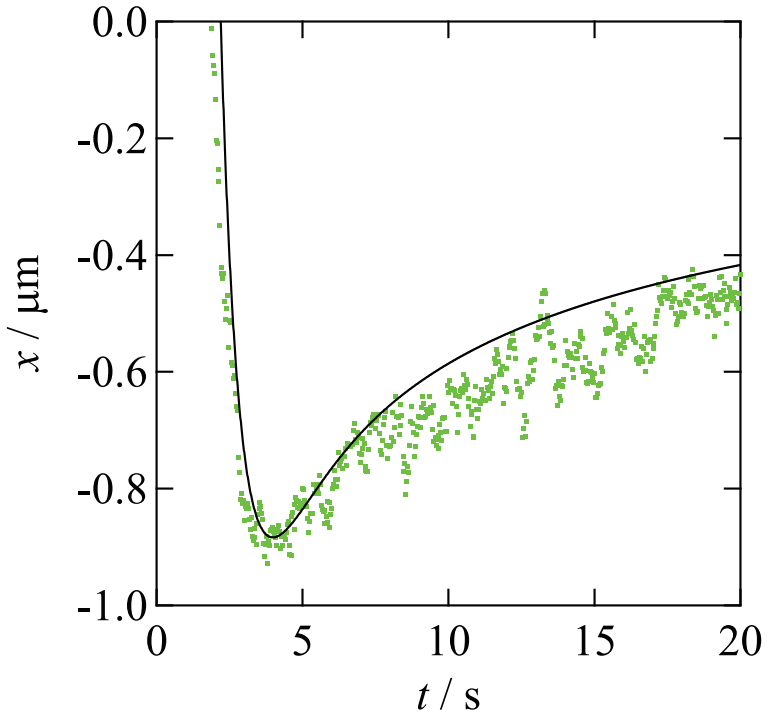

Figure 4.7. Comparison of experimental and simulated trajectories at $V_i = 1.00$ V and $V_f = 2.25$ V.

The resultant line density ρ of a disclination ($V_f = 2.25$ V) is shown in Fig. 4.8. ρ is roughly independent of V_i. This is reasonable because the whole dynamics progresses under V_f. On the other hand, ρ decreased with increasing V_f. The tendency of decreasing ρ was found regardless of the history of applying voltage. These results suggest that ρ is dominated by the voltage at which disclination dynamics occurs.

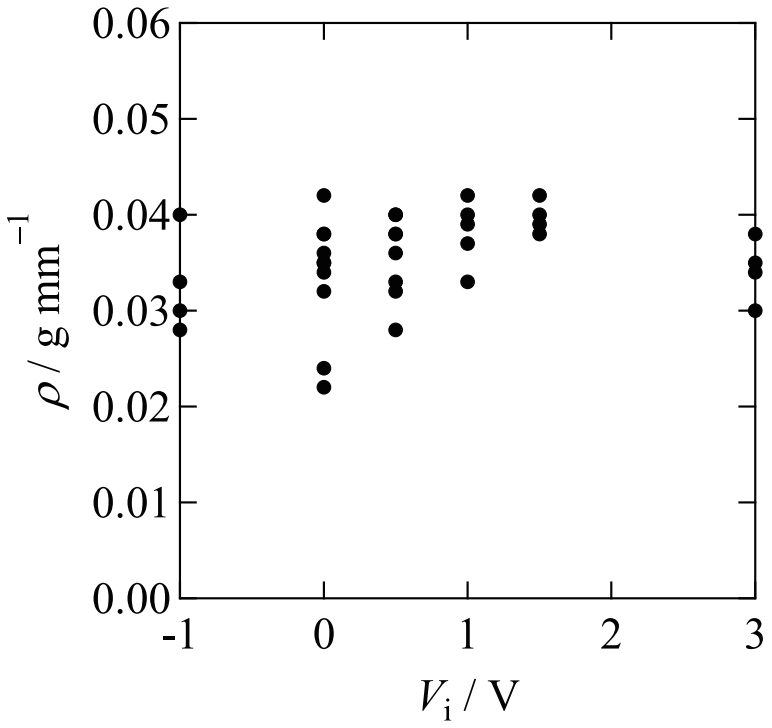

Figure 4.8. Experimental effective line density ρ of the disclination under $V_\mathrm{f} = 2.25$ V as a function of V_i.

4.4 Theoretical Estimation of ρ

The origin and physical meaning of the mass term in Eq. 4.5 are not clear. It was expected, within the elastic theory, that the disclination would have nonzero line density [42]. The elastic energy of the director field is increased around a moving disclination due to viscous stress. Deformation of the director field around a moving disclination is schematically illustrated in Fig. 4.10. Director field of $s = -1$ disclination is shown in Fig. 4.10. for the purpose of illustration. Similar deformation is induced to a $s = -1/2$ disclination. The additional energy of a moving disclination can be treated as the kinetic energy. Since the increment in the elastic energy starts from the quadratic term of velocity by virtue of symmetry, its coefficient can be regarded as $\rho/2$.

At this stage, however, it is noted that the same mass should emerge under both dc and ac cases because the scenario is within the elastic theory. This clearly contradicts the experimental finding. To see to what extent does the scenario works, it would be valuable to estimate the line density of a disclination.

It is necessary to calculate the elastic energy of the director field as a function of velocity. In order to calculate the energy, the director field around a moving disclination is considered. The director

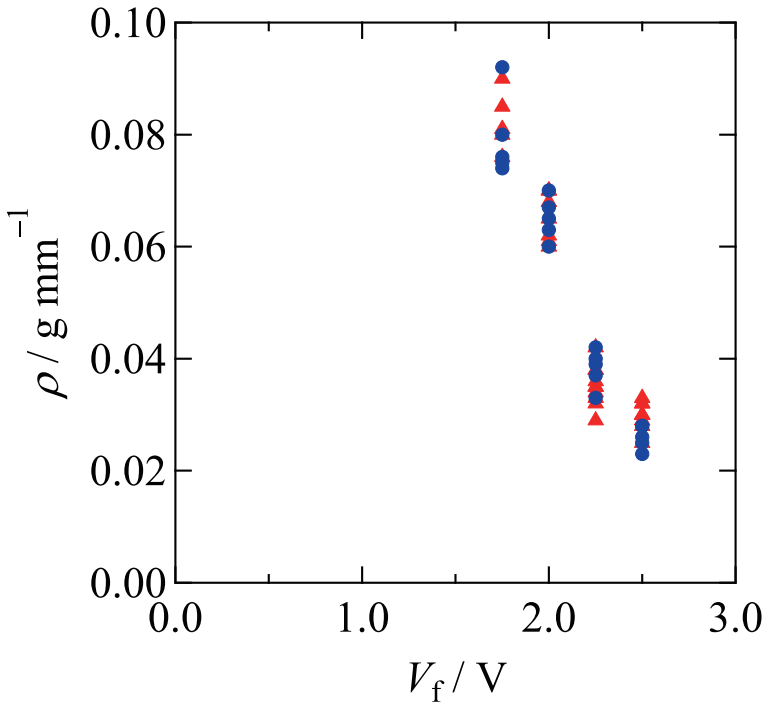

Figure 4.9. Experimental effective line density ρ of a disclination as a function of V_i. ρ depends on applied final voltage V_f. ▲: $V_\mathrm{i} = 0.00$ V. ●: $V_\mathrm{f} - V_\mathrm{i} = 1.25$ V.

field around a moving disclination obeys the following basic equation [13, 14].

$$-K_1 \triangle \varphi + \varepsilon_0 \varepsilon_\mathrm{a} E^2 \sin\varphi \cos\varphi + \gamma_1 v \frac{\partial \varphi}{\partial x} = 0. \tag{4.6}$$

Here γ_1 is rotational viscosity and K_1 an elastic constant. As seen from Eq. 4.6, it is possible to fix a disclination while assuming the stationary flow of the NLC, in stead of considering a moving disclination in stationary NLC without net flow.

In actual calculations, a disclination is fixed on the origin of the system for the easy treatment. The NLC is assumed to be moving at a constant velocity with a stationary elastic field, accordingly. However, the velocity is used as a relative velocity of a disclination with respect to the NLC. The positive velocity means that a disclination moves right. Velocity is set between $-5 \sim +10$ μm/s, which covers the velocities experimentally observed. Applied dc voltage, corresponding to V_f in the experiments, is assumed between $0 \sim 2.5$ V, which covers an actual experimental condition. The

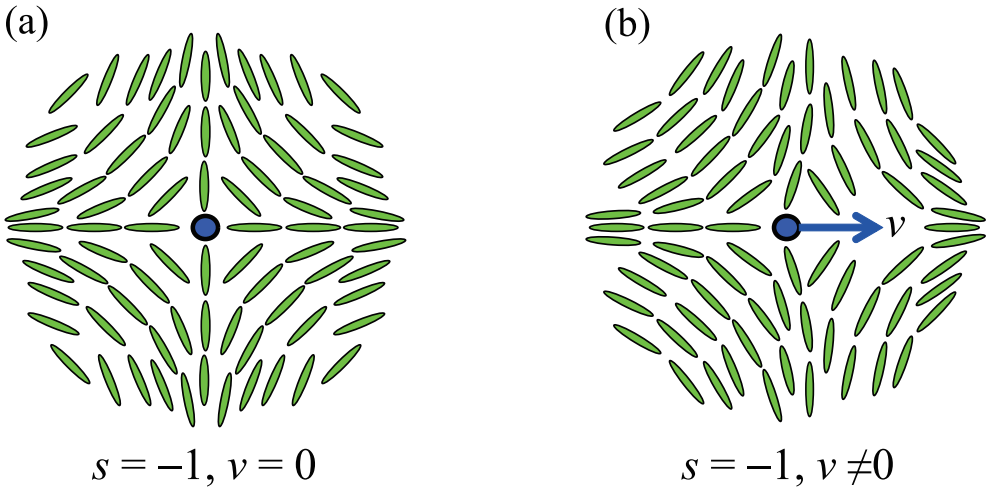

Figure 4.10. Director field around static (a) and moving disclination (b) of $s = -1$. Because of viscous torque, director field around moving disclination is distorted.

boundary condition for an $s = -1/2$ disclination is illustrated in Fig. 4.11, and is expressed as,

$$\varphi(x, d/2) = 0,$$
$$\varphi(x, 0) = \begin{cases} 0 & (x < 0), \\ \pi/2 & (x \geq 0), \end{cases}$$
$$\left.\frac{\partial \varphi}{\partial x}\right|_{x=\pm\infty} = 0.$$

The basic equation is integrated to simulate the director field (director angle φ as a function of the position), assuming $\gamma_1 = 0.0447$ Pa s(of 8CB at 39.0 °C), and $K_1 = 4.48$ pN [37]. Director angle $\varphi(x,z)$ is calculated in a domain of $z \geq 0$. Since φ is symmetric with respect to the x-axis, φ for $z < 0$ is given as the mirror image. Cell gap d is set to be 50 μm to mimic the experimental setup ($d = 55$ μm). φ is obtained by using Gauss-Seidel method on a square mesh (0.1 μm) in the area of $-100 \leq x/\mu\text{m} \leq 100$ and $0 \leq z/\mu\text{m} \leq 25$. Since the size along x direction is large enough in comparison with characteristic lengths of director deformation: Characteristic length of deformation is decided by electric field and substrate. When an electric field is applied to the system, the electric coherence length ξ_E is given as a function of applied field. It is a characteristic length, over which the angle of director changes from $\varphi = 0$ on the surface to $\varphi = \pi/2$ in the bulk NLC area. Typical length of ξ_E is about 10 μm in our experiment. Another characteristic length is a half of cell gap $d/2$. This is also the length of the director deformation from $\varphi = 0$ on the surface to $\varphi = \pi/2$ in the bulk. System size along x direction is large enough compared to ξ_E and $d/2$. The present simulation thus

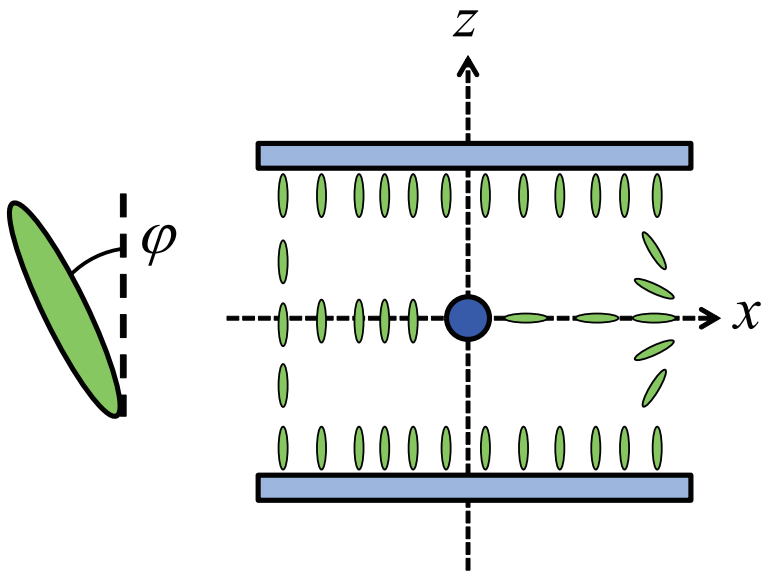

Figure 4.11. Schematic illustration of boundary condition, written as Eq. 4.4. Disclination is put on the origin of the *xz*-plane.

approximates an ideal system with an infinite size along the x direction.

Director field around an $s = -1$ disclination is also simulated in a similar system with the boundary condition

$$\varphi(x,0) = \begin{cases} -\pi/2 & (x < 0), \\ \pi/2 & (x \geq 0). \end{cases}$$

Other conditions for the simulation are the same as the case of an $s = -1/2$ disclination.

The energy density (per unit volume) is divided into elastic energy f_{e} and dielectric energy f_{el}. The energy density is thus given by,

$$f_{\mathrm{total}} = f_{\mathrm{e}} + f_{\mathrm{el}} = \frac{K_1}{2}\nabla^2\varphi - \frac{1}{2}\varepsilon_0\varepsilon_{\mathrm{a}}E^2\cos^2\varphi. \tag{4.7}$$

The total energy of the system is obtained by integrating f_{total} over volume of the whole system. The integration is written as follows.

$$F_{\mathrm{total}} = \int \left[\frac{K_1}{2}\nabla^2\varphi - \frac{1}{2}\varepsilon_0\varepsilon_{\mathrm{a}}E^2\cos^2\varphi\right] dxdz. \tag{4.8}$$

Since this model is assumed to be a two-dimensional system, the energy F_{total} corresponds to the energy of a disclination per unit length (along the y direction).

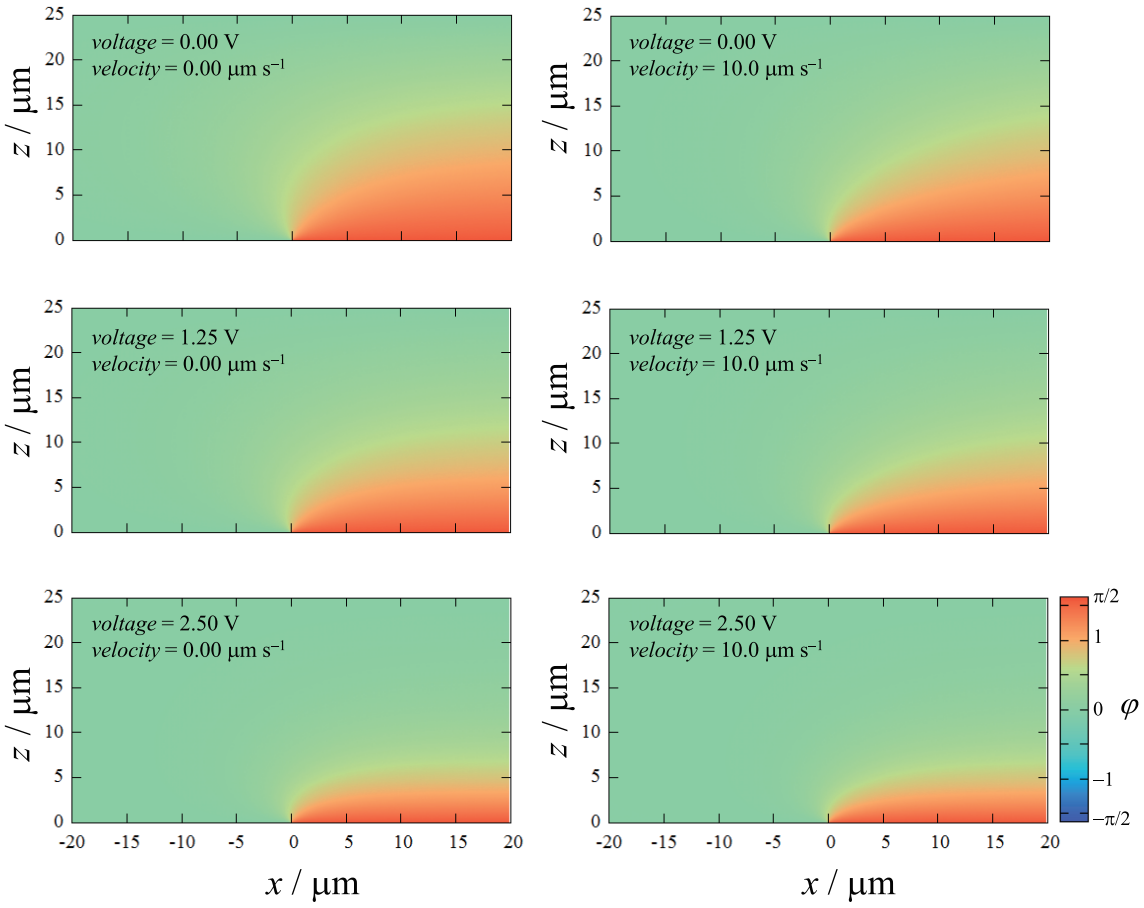

Figure 4.12. Director angle around $s = -1/2$ disclination. φ changes from 0 (green) to $\pi/2$ (red) in these figures. Relation between color and φ is shown in the color bar.

Some results of simulation of φ are shown in Fig. 4.12 and Fig. 4.13 for $s = -1/2$ and $s = -1$, respectively. In both cases, the director field is deformed by applied voltage. Deformation around substrate surface is reduced under voltage, and a director tends to be perpendicular to the surface. When a disclination is moving in the system, the director field is deformed by the motion. The deformation is clearly seen around a $s = -1$ disclination, shown in Fig. 4.13. Since stationary state of the director field obeys the least-energy principle, the deformed director field with velocity v has an excess energy.

Figure 4.14 shows the energy increment as a function of the velocity of a disclination. The state with the least energy is set to be the origin of these plots. Energy increments are plotted against $\Delta v = v - v_0$, where v_0 is the velocity of the least energy state. While a static $s = -1$ disclination has the least energy by virtue of the symmetry, $s = -1/2$ disclination has an asymmetric director field with respect to the y-axis even in a static state. Total energy density is therefore slightly decreases when the $s = -1/2$ disclination moves toward left. The elastic energy at $v = 0$ is not the minimum,

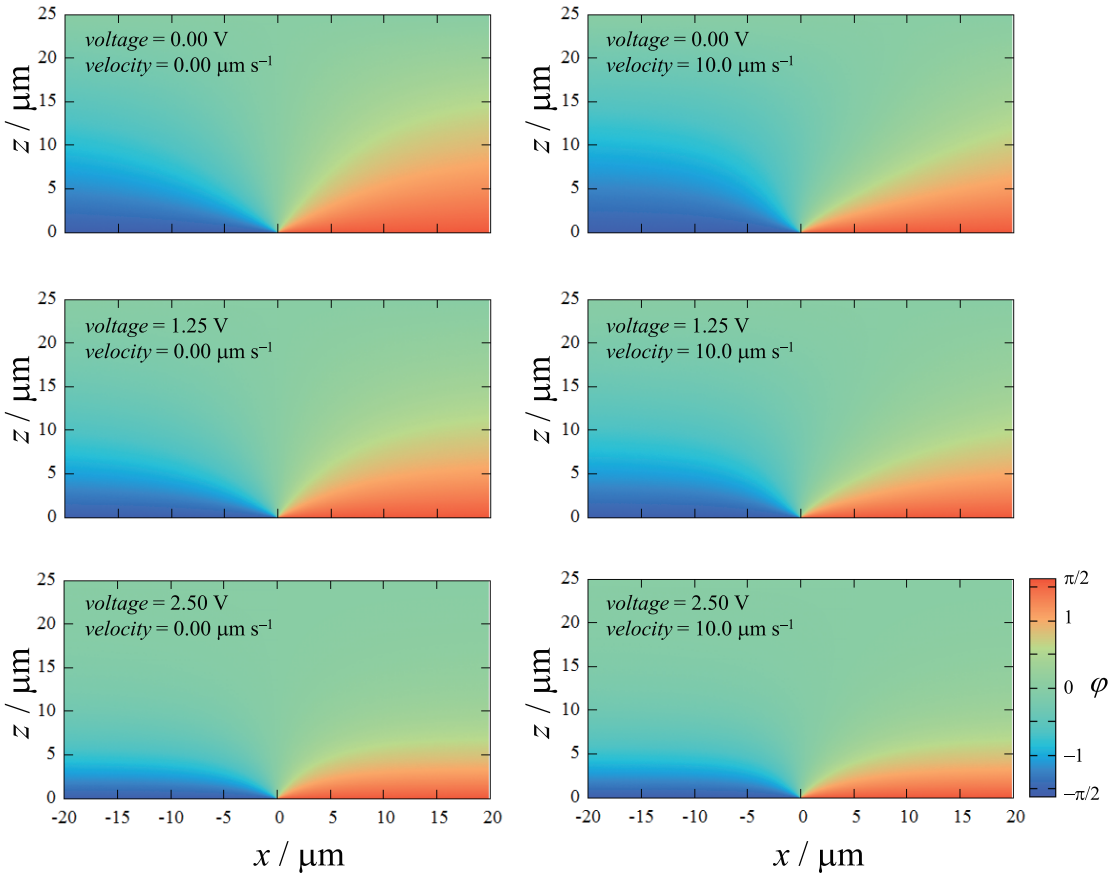

Figure 4.13. Director angle around $s = -1$ disclination. φ changes from $-\pi/2$ (blue) to $\pi/2$ (red) in these figures. Relation between color and φ is shown in the color bar.

accordingly. The dependence is well approximated by a quadratic function of the velocity, regardless of the topological charge s. These results of simulation is fitted to a quadratic function $\Delta F = av^2$. Since a fitting parameter a is regarded as $\rho/2$, the line density ρ is obtained theoretically within the elastic theory.

In Fig. 4.15, the obtained ρ is compared with the experimental results. ρ decreases with increasing voltage. This tendency resembles the experimental results. ρ of a $s = -1$ disclination is estimated by using the same method. ΔF and ρ have the same tendency with that of a $s = -1/2$ disclination. Because the director is caught by an electric field, the deformation of the director field becomes weaker under a stronger field. Therefore, the energy increment ΔF also becomes smaller. This means the coefficient $a = \rho/2$ decreases with increasing electric field. In this way, voltage dependence of theoretical ρ is explained.

The estimate of the effective line density ρ thus obtained is smaller by more than an order of magnitude than the experimental "line density" shown in Fig. 4.15. Experimental result of ρ is several times as large as numerical result of $s = -1$ disclination. This discrepancy clearly indicates that another reasoning(s) are necessary for the observed oscillation than the elastic theory, though the calculated small "line density" may be consistent with the need for assuming small ρ to explain the dynamics under an ac field as an overdamping.

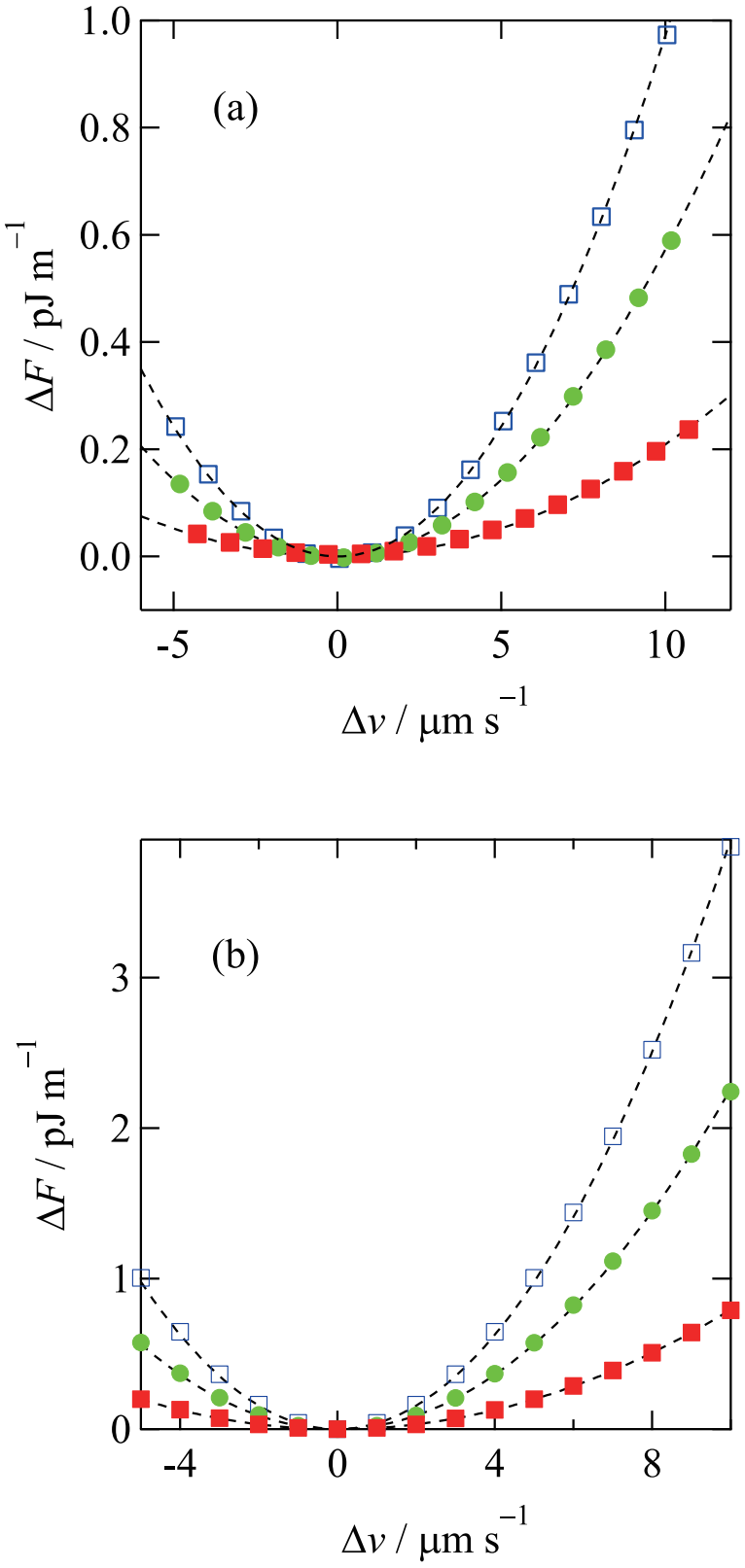

Figure 4.14. Energy increment ΔF of the moving disclination with $s = -1/2$ (a), and $s = -1$ (b). □, 0.00 V; ●, 1.25 V; ■, 2.50 V.

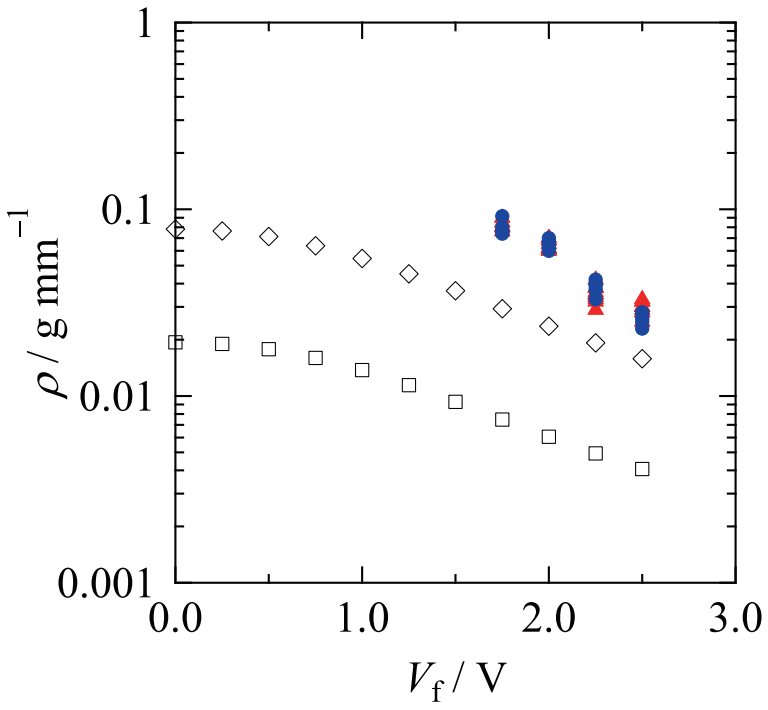

Figure 4.15. Theoretical estimate of ρ for a disclination with $s = -1/2$ (open square) and -1 (open diamond). Filled marks represent experimentally estimated ρ. ▲: $V_i = 0.00$ V. ●: $V_f - V_i = 1.25$ V.

4.5 Discussion

In this chapter, characteristic oscillation dynamics was found after the abrupt switching of the applied dc voltage. On the other hand, the oscillation dynamics was not observed under the 1 kHz ac voltage. Since the dielectric energy of the NLC is proportional to the square of the field strength in the theory, dc and ac fields are indistinctive if the frequency of the ac field is high enough. In the present experiment, the frequency is high enough in comparison with the motion of the disclination, as evidenced by non-synchronous motion with the applied voltage. However, the experimental results shows that the disclination dynamics under the ac voltage is different from that under the dc voltage.

In the present experimental setup, the disclination dynamics may be influenced by the accumulation of charged impurities on the electrode. Under a dc voltage, the applied field may be screened by the accumulation of charged impurities, resulting in a time-dependent effective electric field. In contrast, impurities cannot move towards one electrode under an ac voltage at a sufficiently high frequency. In this respect, ac and dc voltage influence the motion of charged impurities in different way. However, the time dependence of the electric field cannot be the origin of the damped oscillation, because the time scale of the motion of a charged particle (*ca.* 1 s) is much shorter than that of the disclination motion (on the order of 10^2 s). Moreover, the existence of the second and third extrema,

clearly observed with $V_i = -1.00$ V in Fig. 4.3(a), cannot be explained because the accumulation of charged impurities (and the creation of a Debye layer) is certainly an example of one-way dynamics. For the same reason, i.e., the difference in relevant time scales, it is difficult to explain the oscillation in terms of flexoelectricity ($\sim 10^{-6}$ s) and/or the dielectric memory effect ($\sim 10^{-6}$ s). Electro hydrodynamic convection may be another cause of the effect exerted on the disclination dynamics. Since the cutoff electric field depends on the frequency, it seems possible to drive a disclination only under a dc field. However, a pattern assignable to the convection was not observed in the experiments.

There seems to exist a new mechanism that induces the oscillation dynamics under a dc field. It is needed to characterize the oscillation dynamics and the driving force on the disclination, in order to reveal the origin of the oscillation. Figures 4.5 and 4.6 shows that the nonlinear driving force acts on the disclination. The nonlinear force becomes noticeably weak around the equilibrium position, and it decreases moderately when x is positive. Since director field between disclination and air-LC interface is deformed largely, force acting on the disclination is increased when the disclination approaches the air-LC interface. It is important to emphasize that G_0 depends on the displacement x, not a distance from the air-LC interface x'. If the driving force is due to deformation of the director field, G_0 can be a function of the distance x'. Because the volume of deformed region is a function of x', it seems to be natural to expect that G_0 is a function of x'. However, it was experimentally revealed that G_0 depends on x. This fact shows that the volume of deformed area is not an decisive parameter that determines a driving force acting on the disclination. It implies that the observed oscillation dynamics is not due to the elastic energy of the bulk NLC.

The oscillation of disclination was discussed by considering a Newton equation model, in order to characterize the dynamics. The driving force that induces the oscillation is regarded as an inertial force due to the mass term of the equation of motion. Effective line density ρ is a characteristic parameter. The parameter was estimated experimentally, and its V_f dependence was found .

V_f dependence of ρ was reproduced by numerical simulations, which was based on the elastic theory. In this simulation, ρ comes from the elastic energy of the director field. In this sense, the bulk elastic energy is regarded as a source of the driving force in the model. However, numerically estimated ρ was an order of magnitude smaller than experimental results. Therefore, the elastic energy of the bulk NLC is too small to explain experimental results.

In this way, it is thus suggested that a radically new mechanism of NLC system induces the oscillation of a disclination. The elastic theory of the NLC considers the energy by director deformation of whole system. However, experimental and theoretical results of the present study imply that the oscillation dynamics is not induced by the bulk elastic energy. We may have to take into considera-

tion local dynamics of the nematic system. Molecular reorientation around the disclination is one of possible examples of such a mesoscopic dynamics.

Considering the fact that disclination dynamics has frequency dependence of the applied voltage, molecular reorientation after switching may give a driving force to the disclination. Under the dc voltage, 8CB molecule tends to be parallel to the applied voltage. On the other hand, they rotate under the 1 kHz ac voltage [33]. It is possible to imagine that the difference of molecular dynamics influenced the disclination motion. If molecular reorientation process is fast enough, the effect of molecular dynamics may appear in driving force. Actually, Fig. 4.6 shows that G_0 is largely enhanced for $V_\mathrm{f} - V_\mathrm{i} \geq 2.25$ V. When $V_\mathrm{f} - V_\mathrm{i}$ is large enough, a molecule around the disclination rotate and may become parallel to the applied field in a very short time. This fast reorientation process might induce large G_0.

4.6 Conclusion

In conclusion, we found a new type of disclination dynamics. The ultraslow oscillatory dynamics was observed only under a dc voltage and not under a high-frequency ac voltage (1 kHz). The difference between the dc and ac cases is difficult to explain by the established mechanisms of disclination dynamics (the elastic theory of a director field). Since the dynamics under a dc voltage has been reported to be qualitatively the same as that under an ac voltage without abrupt switching of the applied voltage, it can be concluded that the difference emerges upon the abrupt switching of the applied field. A further extensive study is necessary to clarify the mechanism of the ultraslow dynamics found in this study. It is worth pursuing whether there exists a hitherto missed link between molecular dynamics and the deformation of a director field that bridges different hierarchies of matter.

Chapter 5

General Conclusion

Although disclination dynamics under external forces have been investigated in previous works, backflow under the surface anchoring effect had not been taken into consideration. Besides, effects of time-dependent external force had not been investigated in these works. In this work, disclination dynamics under external forces was investigated experimentally. Surface anchoring effect and external electric field were treated as controllable external forces. Disclination dynamics under the force of anchoring effect and the static electric field was discussed in Chapters 2 and 3, respectively. Annihilating dynamics under these forces were analyzed considering the backflow. Effect of the time-dependent external force was discussed in Chapter 4.

In Chapter 2, the annihilation dynamics of disclination pair was investigated. Disclination dynamics was observed in the simplest system where only the strong anchoring worked. Driving force due to the anchoring was treated as a controllable parameter that influenced disclination motion. Relative effect of the anchoring was controlled by changing the cell gap d. Trajectories of disclinations with $s = \pm 1/2$ was recorded, and the velocities of positive and negative disclinations (v_+ and v_-) were analyzed. In a thin LC cells, the disclinations moved at a constant velocity when the distance u between them was large enough, while disclinations were accelerated just before the annihilation in a thick LC cell. Acceleration started earlier in a thicker LC cell. The elastic theory predicts, as a function of d, the increase of ξ_c, the distance within which attractive interaction between disclinations become effective. An $s = \pm 1/2$ disclination was differently accelerated by the backflow in the experimental systems, resulting in an asymmetric annihilation. The velocity of a disclination with $s = -1/2$ was assumed to correspond to the unperturbed one, which should be estimated by the elastic theory. Experimental results were smaller than the theoretical prediction, but both decreased with increasing d. In this way, the cell gap dependence of dynamics were described in the elastic theory.

Velocity ratio v_+/v_- were discussed as a function of d in order to discuss the cell gap dependence

of the backflow. When $d \geq 2$ μm, v_+/v_- was about $1.6 - 2.0$. On the other hand, v_+/v_- rapidly became close to 1, when $d = 1$ μm. This experimental results show that there is a region where the flow is suppressed within 0.5 μm from the cell surface. The director field in the LC cell according to the elastic theory was consistent with that expected for the suppressed flow near the substrates.

In this chapter, the director field in the LC cell was theoretically analyzed by the elastic theory. It was revealed that the suppressed flow region was generated by the anchoring effect. Mechanism of generation of suppressed flow was qualitatively explained by director field in the LC cell.

In Chapter 3, the effect of an electric field was introduced to the system in order to apply a force on a bulk region of NLC. Two electrodes were sandwiched between glass substrates. Electric field was applied horizontally to the surfaces, while perpendicular to the anchoring easy axis.

v_+ and v_- of $\pm 1/2$ disclinations were estimated from experimental trajectories. The dependence on electric field of the velocities was discussed. The velocity decreased with increasing electric field. Since director between disclinations tends to be parallel to electric field, the director field in the region was stabilized by the electric field. In this way, driving force was reduced and disclination velocity became slow. The dependence on electric field of the velocity was successfully rationalized by considering the energy of deformed field.

In order to discuss the backflow in the cell, the velocity ratio v_+/v_- was analyzed against the external field. It is theoretically known that v_+ is roughly twice as fast as v_- because of the backflow in systems where the surface effect is negligible. v_+/v_- was almost independent of applied electric field and v_-. These results imply that the mechanism of generating backflow remains unchanged under an electric field. Flow field is generated only to keep v_+/v_- constant.

Chapter 4 deals with an effect of time-dependent field, in contrast to Chapters 2 and 3, where disclination dynamics under static external field was discussed. From a vast variety of time dependent fields, abrupt switching was chosen as the simplest example.

After switching of applied dc voltage, a kind of damped oscillation of $s = -1/2$ disclination string was observed. On the other hand, any oscillation was not observed after switching of 1 kHz ac voltage: Disclination approached to air-LC interface monotonously. It means that disclination relaxes faster under ac voltage than dc case. Dynamics under the ac voltage could be qualitatively understood within the elastic theory. This difference implies that there is frequency dependence of disclination relaxation.

The oscillation dynamics under dc voltage was examined in detail. To discuss characteristics of the motion, trajectories of oscillations were analyzed. A half of oscillation cycle $(\tau/2)_{\mathrm{app}}$ was estimated as the interval between crossing the equilibrium position. $(\tau/2)_{\mathrm{app}}$ depended on the amplitude of the

oscillation. It implies that nonlinear driving force acts on the disclination. Nonlinearity of the driving force was discussed by estimating it from experimental results. It was found that the force field can be expressed as a smooth nonlinear function of amplitude x_{ex} when the jump in voltages between final and initial states ($|V_f - V_i|$) is smaller than 2.25 V.

A Newton equation was applied as a minimal phenomenological model to describe the oscillation of a disclination. An effective line density ρ was introduced to write the equation of motion. Numerically simulated trajectory was partially fitted to experimental results by setting suitable ρ. While resultant ρ decreased with increasing V_f, it was independent of V_i, implying that ρ was decided by the voltage under which disclination dynamics progressed.

Possible origin of ρ was examined within the elastic theory. Disclination dynamics accompanies energy increment ΔF, which can be regarded as the kinetic energy of the disclination, $\rho v^2/2$. Within the elastic theory, elastic energy under a constant voltage was estimated numerically as a function of velocity v of a disclination. ρ estimated by this scenario decreased with increasing voltage. Although this tendency was consistent with experimental results, theoretically estimated ρ was an order of magnitude smaller than experimental ones. It was thus revealed that the elastic energy of NLC is too small to explain the oscillation of disclination.

Experimental results imply that there is some interrelation between local dynamics of NLC and a driving force acting on the disclination. Driving force may be generated by local reorientation process of mesogenic molecules (8CB in the present experiments) around the disclination core. Disclination oscillation seems to be a fundamentally new dynamics in non-equilibrium state.

In conclusion, I investigated disclination dynamics under external forces. These forces were introduced by surface anchoring and electric field. Annihilation dynamics of positive and negative disclination pair was observed under static external force, and discussed considering the backflow effect. It was revealed that dynamics under static forces could be explained by existing theoretical description within the continuum theory of NLC. On the other hand, a fundamentally new dynamics was found in the non-equilibrium relaxation process, after an abrupt switching of the external field. It is expected that new kinds of mechanisms for disclination dynamics will be found by investigating motions under time-dependent external forces. Relation between local molecular dynamics and macroscopic dynamics in LC (including disclination motion) may be revealed. The present investigation should hopefully be the first step towards such a new stage of LC science.

References

[1] S. Chandrasekhar, *Liquid Crystals*, 2nd ed. (Cambridge University Press, Cambridge, 1992).

[2] P. G. de Gennes and J. Prost, *The Physics of Liquid Crystals*, 2nd ed. (Oxford Science Pubrications, Oxford, 1993).

[3] P. M. Chaikin and T. C. Lubensky, *Principles of Condensed Matter Physics*, (Cambridge University Press, Cambridge, 1995).

[4] N. D. Mermin, *Rev. Mod. Phys.*, **51**, 591 (1979).

[5] F. C. Frank, *Discuss. Faraday. Soc.*, **25**, 19 (1958).

[6] A. Pargellis, N. Turok, and B. Yurke, *Phys. Rev. Lett.*, **67**, 1570 (1991).

[7] I. Chuang, N. Turok, and B. Yurke, *Phys. Rev. Lett.*, **66**, 2472 (1991).

[8] T. Nagaya, H. Hotta, H. Orihara, and Y. Ishibashi, *J. Phys. Soc. Jpn.*, **60**, 1572 (1991).

[9] T. Nagaya, H. Hotta, H. Orihara, and Y. Ishibashi, *J. Phys. Soc. Jpn.*, **61**, 3511 (1992).

[10] P. Cladis, W. van Saarloos, P. Finn, and A. Kortan, *Phys. Rev. Lett.*, **58**, 222 (1987).

[11] G. Ryskin and M. Kremenetsky, *Phys. Rev. Lett.*, **67**, 1574 (1991).

[12] A. Bogi, P. Martinot-Lagarde, I. Dozov, and M. Nobili, *Phys. Rev. Lett.*, **89**, 225501 (2002).

[13] K. Minoura, Y. Kimura, K. Ito, and R. Hayakawa, *Phys. Rev. E*, **58**, 643 (1998).

[14] P. Biscari and T. J. Sluckin, *J. Appl. Math.*, **65**, 2141 (2005).

[15] V. Frederiks and V. Tsvetkov, *Phy. Z. Soviet. Union.*, **6**, 490 (1934).

[16] G. Tóth, C. Denniston, and J. M. Yeomans, *Phys. Rev. Lett.*, **88**, 105504 (2002).

[17] D. Svenšek and S. Žumer, *Phys. Rev. E*, **66**, 021712 (2002).

[18] C. Blanc, D. Svenšek, S. Žumer, and M. Nobili, *Phys. Rev. Lett.*, **95**, 097802 (2005).

[19] A. M. Sonnet, *Continuum Mech. Thermodyn.*, **17**, 287 (2005).

[20] A. M. Sonnet and E. G. Virga, *Liq. Cryst.*, **36**, 1185 (2009).

[21] P. Biscari and T. J. Sluckin, *Eur. J. Appl. Math.*, **23**, 181 (2012).

[22] C. Denniston, *Phys. Rev. B*, **54**, 6272 (1996).

[23] G. Tóth, C. Denniston, and J. M. Yeomans, *Phys. Rev. E*, **67**, 051705 (2003).

[24] K. Skarp, S. T. Lagerwall, and B. Stebler, *Mol. Cryst. Liq. Cryst.*, **60**, 215 (1980).

[25] J. Bunning, T. Faber, and P. Sherrell, *J. Physique.*, **42**, 1175 (1981).

[26] J. Brugués, J. I. Mullol, J. Casademunt, and F. Sagués, *Phys. Rev. Lett.*, **100**, 037801 (2008).

[27] P. Oswald and J. Ignés-Mullol, *Phys. Rev. Lett.*, **95**, 027801 (2005).

[28] W. Helfrich, *J. Chem. Phys.*, **51**, 4092 (1969).

[29] S. Kai, K. Yamaguchi. and K. Hirakawa, *Jpn. J. Appl. Phys.*, **14**, 1653 (1975).

[30] M. I. Barnik, L. M. Blinov, S. A. Pikin, and A. N. Trufanov, *Sov. Phys. JETP.*, **45**, 396 (1977).

[31] K. Negita, *J. Chem. Phys.* **105**, 7873 (1996).

[32] T. Yanagimachi, S. Yasuzuka, Y. Yamamura, and K. Saito, *J. Phys. Soc. Jpn.*, **81**, 034601 (2012).

[33] M. Y. Jin and J. J. Kim, *J. Phys.: Condens. Matter*, **13**, 4435 (2001).

[34] J. Ignés-Mullol, J. Baudry, L. Lejcek, and P. Oswald, *Phys. Rev. E*, **59**, 568 (1999).

[35] H. Kneppe, F. Schneider, and N. Sharma, *J. Chem. Phys.*, **77**, 3203 (1982).

[36] H. Kneppe, F. Schneider, and N. Sharma, *Phys. Chem.*, **85**, 784 (1981).

[37] M. Bradshaw, E. Raynes, J. Bunning, and T. Faber, *J. Physique*, **46**, 1513 (1985).

[38] B. Ratna and R. Shashidhar, *Mol. Cryst. Liq. Cryst.*, **42**, 113 (1977).

[39] B. Gettelfinger, F. Hung, J. Ortiz, O. Guzman, A. Rey, N. Abbott, and J. De Pablo, *DYNA-Colombia*, **75**, 185 (2008).

[40] A. Mertelj and M. Čopič, *Phys. Rev. E*, **69**, 021711 (2004).

[41] N. Osterman, J. Kotar, E. Terentjev, and P. Cicuta, *Phys. Rev. E*, **81**, 061701 (2010).

[42] H. Pleiner, *Phys. Rev. A*, **37**, 3986 (1988).

List of publications

- Chapter 2.

  T. Yanagimachi, S. Yasuzuka, Y. Yamamura, and K. Saito, “Cell Gap Dependence of Nematic Backflow around Annihilating Disclination Pair”, *J. Phys. Soc. Jpn.*, **81**, 074603 (2012).

- Chapter 3.

  T. Yanagimachi, S. Yasuzuka, Y. Yamamura, and K. Saito, “Backflow-Induced Asymmetric Annihilation of Nematic Disclinations under Strong Anchoring Condition”, *J. Phys. Soc. Jpn.*, **81**, 034601 (2012).

- Chapter 4.

  T. Yanagimachi, M. Hishida, Y. Yamamura, and K. Saito, “Ultraslow Oscillation of Nematic Disclination after Abrupt Switching of dc Voltage”, accepted for publication in *J. Phys. Soc. Jpn.*